

NASA/TP-2005-213531



Robust Control Design for Systems With Probabilistic Uncertainty

Luis G. Crespo
National Institute of Aerospace, Hampton, Virginia

Sean P. Kenny
Langley Research Center, Hampton, Virginia

March 2005

The NASA STI Program Office ... in Profile

Since its founding, NASA has been dedicated to the advancement of aeronautics and space science. The NASA Scientific and Technical Information (STI) Program Office plays a key part in helping NASA maintain this important role.

The NASA STI Program Office is operated by Langley Research Center, the lead center for NASA's scientific and technical information. The NASA STI Program Office provides access to the NASA STI Database, the largest collection of aeronautical and space science STI in the world. The Program Office is also NASA's institutional mechanism for disseminating the results of its research and development activities. These results are published by NASA in the NASA STI Report Series, which includes the following report types:

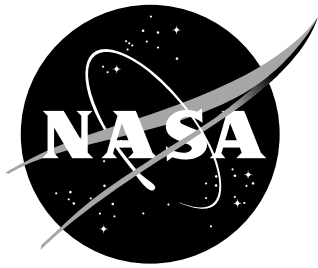
- **TECHNICAL PUBLICATION.** Reports of completed research or a major significant phase of research that present the results of NASA programs and include extensive data or theoretical analysis. Includes compilations of significant scientific and technical data and information deemed to be of continuing reference value. NASA counterpart of peer-reviewed formal professional papers, but having less stringent limitations on manuscript length and extent of graphic presentations.
- **TECHNICAL MEMORANDUM.** Scientific and technical findings that are preliminary or of specialized interest, e.g., quick release reports, working papers, and bibliographies that contain minimal annotation. Does not contain extensive analysis.
- **CONTRACTOR REPORT.** Scientific and technical findings by NASA-sponsored contractors and grantees.
- **CONFERENCE PUBLICATION.** Collected papers from scientific and technical conferences, symposia, seminars, or other meetings sponsored or co-sponsored by NASA.
- **SPECIAL PUBLICATION.** Scientific, technical, or historical information from NASA programs, projects, and missions, often concerned with subjects having substantial public interest.
- **TECHNICAL TRANSLATION.** English-language translations of foreign scientific and technical material pertinent to NASA's mission.

Specialized services that complement the STI Program Office's diverse offerings include creating custom thesauri, building customized databases, organizing and publishing research results ... even providing videos.

For more information about the NASA STI Program Office, see the following:

- Access the NASA STI Program Home Page at <http://www.sti.nasa.gov>
- E-mail your question via the Internet to help@sti.nasa.gov
- Fax your question to the NASA STI Help Desk at (301) 621-0134
- Phone the NASA STI Help Desk at (301) 621-0390
- Write to:
NASA STI Help Desk
NASA Center for AeroSpace Information
7121 Standard Drive
Hanover, MD 21076-1320

NASA/TP-2005-213531



Robust Control Design for Systems With Probabilistic Uncertainty

Luis G. Crespo
National Institute of Aerospace, Hampton, Virginia

Sean P. Kenny
Langley Research Center, Hampton, Virginia

National Aeronautics and
Space Administration

Langley Research Center
Hampton, Virginia 23681-2199

March 2005

Acknowledgments

This work was supported by the National Aeronautics and Space Administration under NASA Contract No. NAS1-97046 while Dr. Crespo was in residence at the National Institute of Aerospace. The authors would like to thank Dr. Daniel Giesy, Dr. Lucas Horta and Dr. Suresh Joshi for their diligence in the review of this manuscript.

Available from:

NASA Center for AeroSpace Information (CASI)
7121 Standard Drive
Hanover, MD 21076-1320
(301) 621-0390

National Technical Information Service (NTIS)
5285 Port Royal Road
Springfield, VA 22161-2171
(703) 605-6000

Abstract

This paper presents a reliability- and robustness-based formulation for robust control synthesis for systems with probabilistic uncertainty. In a reliability-based formulation, the probability of violating design requirements prescribed by inequality constraints is minimized. In a robustness-based formulation, a metric which measures the tendency of a random variable/process to cluster close to a target scalar/function is minimized. A multi-objective optimization procedure, which combines stability and performance requirements in time and frequency domains, is used to search for robustly optimal compensators. Some of the fundamental differences between the proposed strategy and conventional robust control methods are: (i) unnecessary conservatism is eliminated since there is not need for convex supports, (ii) the most likely plants are favored during synthesis allowing for probabilistic robust optimality, (iii) the tradeoff between robust stability and robust performance can be explored numerically, (iv) the uncertainty set is closely related to parameters with clear physical meaning, and (v) compensators with improved robust characteristics for a given control structure can be synthesized.

Several numerical methods for estimation, including the Hammersley sequence sampling method, the First Order Reliability method, and the First- and Second-Moment-Second-Order-Methods, are compared. Examples using output-feedback and full-state feedback with state estimation are used to demonstrate and validate the methodology.

Contents

Abstract	iii
Contents	v
List of figures	vii
List of tables	viii
Nomenclature	ix
1 Introduction	1
2 System Dynamics	2
3 Reliability-Based Metrics	4
3.1 Random Variables	4
3.2 Random Processes	5
3.3 Realizations	6
3.3.1 Robust Stability	6
3.3.2 Time-Domain	7
3.3.3 Frequency-Domain	8
3.4 Reliability Bounds	8
4 Robustness-Based Metrics	9
5 Numerical Estimation	10
5.1 Hammersley-Sequence-Sampling (HSS)	10
5.2 Mean and Variances	11
5.2.1 Sampling	12
5.2.2 First and Second Moments of a Second Order Taylor approx- imation (FSMSO)	12
5.3 Failure probabilities	13
5.3.1 Sampling	13
5.3.2 First-Order-Reliability-Method (FORM)	13
5.3.3 Hybrid Approach	14
6 Control Synthesis	15
6.1 Reliability-based	15
6.1.1 Robustness Considerations	15
6.2 Robustness-based	16
6.3 Multi-objective Optimization	17
6.4 Synthesis Procedure	17
6.5 Optimization under Uncertainty	18

7	Numerical Examples	19
7.1	Satellite Attitude Control	19
7.1.1	Nominal Compensator	20
7.1.2	Reliability-based compensator	20
7.1.3	Using Mean and Variance based metrics	23
7.2	Disturbance Rejection for a Flexible Beam	29
7.2.1	Nominal Compensator	32
7.2.2	Reliability-based Compensator	32
7.2.3	Mixed Compensator	33
7.2.4	Mean and Variance based Compensator	34
8	Conclusions	35
	References	37

List of Figures

1	Sketch of the reliability metric for x	5
2	Sketch of the reliability metric for $x(h)$	7
3	Points and samples via MCS and HSS.	12
4	Robust performance concepts and shapable failure domains	16
5	CDF of λ for the nominal compensator.	21
6	$y(t)$ for the nominal compensator. A zoom is shown below.	21
7	$u(t)$ for the nominal compensator.	22
8	CDF of λ for the reliability-based optimal compensator.	23
9	$y(t)$ for the reliability-based optimal compensator. A zoom is shown below.	24
10	$u(t)$ for the reliability-based optimal compensator.	25
11	Bode plot of the loop gain for the reliability-based optimal compensator.	25
12	CDFs of λ	26
13	CDF of λ for the mean and variance based compensator.	26
14	$y(t)$ for the mean and variance based compensator. A zoom is shown below.	27
15	$u(t)$ for the mean and variance base compensator	28
16	CDF of λ for a compensator with parameters \mathbf{k}_4	30
17	$y(t)$ for a compensator with parameters \mathbf{k}_4 . A zoom is shown below.	30
18	$u(t)$ for a compensator with parameters \mathbf{k}_4	31
19	Flexible beam test article.	31
20	PDFs for the reliability based and the robustness based compensators.	33
21	Bode diagrams of T_{zy} for \mathbf{d}_2	34
22	CDFs of λ for \mathbf{d}_3 and \mathbf{d}_4	35

List of Tables

1	Uncertainty Model.	20
2	Comparison of HSS and FSMSO for \mathbf{k}_3	29
3	Uncertainty Model.	32

Nomenclature

A_1	First assessment of the compensator
A_2	Second assessment of the compensator
\mathcal{A}	Admissible domain
\mathbf{A}	State space matrix
b	Bound of r
\underline{b}	Bound of \underline{r}
\bar{b}	Bound of \bar{r}
B	Beta probability distribution
\mathbf{B}	State space matrix
\mathbf{c}	Cost vector
\mathbf{C}	State space matrix
\mathbf{d}	Design variable
\mathbf{d}^*	Reliability optimal design
\mathbf{D}	State space matrix
e	Number of h -samples.
\mathbf{e}	Parameter of the failure boundary
$E[\cdot]$	Expected value operator
E	Young modulus
\mathbf{E}	State space matrix
$f(\cdot)$	Probability density function (PDF)
$f(\cdot, \cdot)$	Parameterized family of PDFs
$F(\cdot)$	Cumulative distribution function (CDF)
$F(\cdot, \cdot)$	Parameterized family of CDFs
$F[\cdot]$	Fourth central moment operator
\mathcal{F}	Failure domain
\mathbf{F}	State space matrix
g	Limit state function
\mathbf{g}	Estimation error
G	Plant transfer function
\mathbf{G}	Feedback gain
h	Arbitrary parameter of a random process
\mathcal{H}	Heaviside function
$\mathcal{I}(\cdot)$	Binary indicator function
J	Cost function
J_e	Estimated value of the cost function
K	Compensator transfer function
\mathbf{k}	Compensator parameters
\mathbf{L}	Observer gain
\mathbf{m}	Hammersley point
\mathcal{M}	Plant
n	Number of samples
N	Normal probability distribution
\mathbf{p}	Uncertain vector parameter
$P[\cdot]$	Probability operator

P_f	Probability of failure
P_{ref}	Reference failure probability
q	Magnitude of the loop transfer function
\mathbf{q}	Uncorrelated standard normal variable
\mathbf{q}^*	Most probable point (MPP)
\mathbf{Q}	State covariance
r	Reliability cost metric
\bar{r}	Reliability metric measuring the violation of the upper failure boundary
\underline{r}	Reliability metric measuring the violation of the lower failure boundary
$\Re[\cdot]$	Real part operator
s	Closed loop pole
\mathbf{S}	Spectral density Matrix
t	Time
T_{zy}	Transfer function from \mathbf{z} to \mathbf{y}
$T[\cdot]$	Third central moment operator
\mathbf{T}	Transformation from \mathbf{q} to \mathbf{p} space
u_{max}	Control saturation bound
U	Uniform probability distribution
\mathbf{u}	Control input
$V[\cdot]$	Variance operator
\mathbf{v}	Sensor noise
\mathbf{w}	Weighting vector
x	Arbitrary random variable dependent on \mathbf{p}
$x(h)$	Arbitrary random process dependent on \mathbf{p}
\mathbf{x}	System state
\mathbf{y}	System output
\mathbf{z}	Process noise
∂	Referring to derivatives with respect to an uncertain parameter
δ	Small perturbation
$\delta(\cdot)$	Dirac delta function
Δ	Support
ϵ	Admissible probability of failure
κ	Time offset
γ	Failure size penalizing function
λ	Random variable used for stability
ω	Frequency
ω_f	Natural frequency of low-pass filter
ϕ_R	R inverse radix number operator
Φ	CDF of a standard normal variable
ρ	Density
τ	Robustness metric
ξ	Dummy variable
ξ_i	Damping ratio of the i th mode
ξ_f	Damping ratio of the low-pass filter
<u>Superscript</u>	
T	Transpose

Subscript

c Referring to the state space representation of the compensator

e Referring to the estimated value

i Referring to the i th sample or point

(i) Referring to the i th component of a vector

rms Referring to the stationary root mean square value

x Referring to the random variable x

$x(h)$ Referring to the random process $x(h)$

Overprint

\wedge Referring to a target value or function

\sim Referring to closed-loop

\cdot Referring to time derivative

$-$ Referring to the upper failure boundary

Underprint

$-$ Referring to the lower failure boundary

1 Introduction

Achieving balance between stability and performance in the presence of uncertainties is one of the fundamental challenges faced by control engineers. Tradeoffs must be made to reach acceptable levels of stability and performance with adequate robustness to parameter uncertainty. These tradeoffs are explicitly linked to the control engineer's choice of uncertainty model as well as how that model is exploited in the synthesis process. Usually, the assumed uncertainty model has a profound impact on the performance robustness of the closed-loop system.

Several uncertainty models, such as norm-bounded perturbations, interval analysis, fuzzy sets and probabilistic methods [1–3] are typically used. The most commonly used robust control methods [4] are μ -synthesis and H -infinity. In these methods, uncertainty is modeled with norm-bounded complex perturbations of arbitrary structure about a nominal plant. This treatment is used primarily because it leads to a tractable set of sufficient conditions for robust stability, making the approach computationally efficient. These methods are based on the most pessimistic value of performance among the possible ones, usually referred to as “worst-case”. This worst-case performance is usually realized only by a single member of the uncertain model set and by a particular input signal. No information is provided regarding the likelihood that this worst-case will ever occur in practice. In addition, the intrinsic mathematical requirements of the approach usually lead to conservative models of uncertainty, over-conservative designs and complicated compensators.

Probabilistic uncertainty not only defines a set of plants where the actual dynamic system is assumed to reside but also associates a weight, the value of the probability density function, to each member of the set. In contrast to conventional robust control methods, this “additional dimension” allows the pursuit of robustly optimal solutions in the probabilistic sense. For instance, reliability-based design searches for solutions that minimize the probability of violating design requirements prescribed in terms of inequality constraints. Hence, reliability-based control design searches for the compensator that places as much probability as possible within the region where the design requirements are satisfied. Notice that this allows the search for the compensator with the best robustness for a given control structure, e.g., the most robust PID controller, even though the violation of some the design requirements for some of the plants in the uncertainty set is possibly unavoidable.

Synthesis approaches based on random searches [5–7] and stochastic gradient algorithms [8–10] have been applied to probabilistic robust control. In these studies, random sampling is the primary tool for assessing and pursuing acceptable levels of robustness in the control solution. On the other hand, asymptotic approximations [11, 12] for the estimation of failure probabilities have only been used as a control analysis tool. The works [5–7, 13, 14] and references cited therein are especially relevant to this paper. Even though they lay down the basic framework for the reliability control synthesis of engineering problems, important aspects of the formulation and of the solution method remain to be explored and refined. This article addresses and extends some of those aspects.

The main contributions of this study to the state of the art in the subject are as follows:

1. The use of robustness-based metrics for minimizing the performance degradation caused by uncertainty.
2. The use of bounds on the reliability metrics based on the first two order moments. This practice reduces considerably the computational demands of the synthesis algorithms based on the estimation of failure probabilities.
3. The use of shapable failure domains within the reliability formulation. This allows the integration of robustness considerations into the conventional reliability approach.
4. The integrated use of deterministic sampling and asymptotic approximations for the estimation of reliability metrics. This hybrid approach (i) reduces the computational complexity of the synthesis algorithm without compromising the accuracy of the results, (ii) eliminates the random character of the estimation, and (iii) eliminates the high computational demands associated with the estimation of small failure probabilities via sampling.

This paper is organized as follows. Section 2 presents basic concepts related to control and probabilistic uncertainty. Section 3 introduces reliability metrics for random variables and processes and presents realizations to stability and time- and frequency-dependent performance metrics. Mean and variance based bounds to the reliability metrics are also derived therein. Robustness-based metrics for random variables and processes are introduced in Section 4. Section 5 presents the numerical methods used to estimate the above mentioned metrics. The control synthesis procedure is presented in Section 6, where specifics of both the reliability and the robustness-based formulations are examined. Two examples are presented in Section 7, where a satellite's attitude control problem and the disturbance rejection in a flexible beam are used to demonstrate the method. Finally, some conclusions are stated in Section 8.

2 System Dynamics

Let \mathbf{p} be a vector of random variables used to model the uncertain parameters of the system. In this study, \mathbf{p} is prescribed *a priori* by the joint probability density function (PDF) $f_{\mathbf{p}}(\mathbf{p})$ or equivalently by the cumulative distribution function (CDF) $F_{\mathbf{p}}(\mathbf{p})$ ¹. The set of values that \mathbf{p} could take, called the *support* of \mathbf{p} , will be denoted as $\Delta_{\mathbf{p}}$.

Consider the probabilistic model $\mathcal{M}(\mathbf{p})$ of a Linear Time Invariant (LTI) system, where the dependence of the model on the uncertain parameters could be non-linear. The reader must notice however, that the developments presented herein do not require the system to be LTI. The propagation of $\Delta_{\mathbf{p}}$ through \mathcal{M} leads to a set

¹In these expressions, the subscript refers to the symbol used for the random variable while the value in parenthesis refers to a particular realization of it.

of uncertain plant models in which the physical system is assumed to reside. The probability distribution of a plant within this set is fully determined by $\mathcal{M}(\mathbf{p})$ and $f_{\mathbf{p}}(\mathbf{p})$. In a transfer function representation, we will refer to the uncertain plant as $G(\mathbf{p})$ and to the compensator as $K(\mathbf{k})$, where \mathbf{k} is the vector of design parameters to be determined. Alternatively, a state space realization of $\mathcal{M}(\mathbf{p})$ leads to

$$\dot{\mathbf{x}} = \mathbf{A}(\mathbf{p})\mathbf{x} + \mathbf{B}(\mathbf{p})\mathbf{u} + \mathbf{F}(\mathbf{p})\mathbf{z} \quad (1)$$

$$\mathbf{y} = \mathbf{C}(\mathbf{p})\mathbf{x} + \mathbf{D}(\mathbf{p})\mathbf{u} + \mathbf{E}(\mathbf{p})\mathbf{v} \quad (2)$$

where \mathbf{x} is the state, \mathbf{u} is the control, \mathbf{z} is process noise, \mathbf{y} is the system output and \mathbf{v} is sensor noise. The noise signals are commonly modeled as delta correlated Gaussian white noises satisfying $E[\tilde{\mathbf{z}}] = \mathbf{0}$ and $E[\tilde{\mathbf{z}}(t)\tilde{\mathbf{z}}^T(t + \kappa)] = \mathbf{S}\delta(\kappa)$, where $\tilde{\mathbf{z}} = [\mathbf{z}^T, \mathbf{v}^T]^T$, \mathbf{S} is the spectral density matrix and $E[\cdot]$ is the expected value operator. In what follows, the explicit dependence on \mathbf{p} is omitted while \mathbf{D} is assumed to be zero.

Important properties used in control design, such as pole placement and the Separation Principle, do not hold due to the offset between the deterministic mathematical model and the actual dynamic system. The effects of parametric uncertainty on the Separation Principle are considered next. For the full-state feedback law $\mathbf{u} = -\mathbf{G}\mathbf{x}$ and a full-order observer with gain \mathbf{L} based on the expected plant $E[\mathcal{M}(\mathbf{p})]$ (any other deterministic plant such as $\mathcal{M}(E[\mathbf{p}])$ could be used instead), the observer equation and the closed-loop dynamics for velocity feedback are given by

$$\dot{\hat{\mathbf{x}}} = (E[\mathbf{A}] - E[\mathbf{B}]\mathbf{G} + \mathbf{L}(\mathbf{C} - E[\mathbf{C}])) \hat{\mathbf{x}} \quad (3)$$

$$\dot{\tilde{\mathbf{x}}} = \tilde{\mathbf{A}}\tilde{\mathbf{x}} + \tilde{\mathbf{B}}\tilde{\mathbf{z}} \quad (4)$$

$$\tilde{\mathbf{y}} = \tilde{\mathbf{C}}\tilde{\mathbf{x}} + \tilde{\mathbf{E}}\tilde{\mathbf{z}} \quad (5)$$

$$\tilde{\mathbf{A}} = \left[\begin{array}{c|c} \mathbf{A} - \mathbf{B}\mathbf{G} & \mathbf{B}\mathbf{G} \\ \hline \mathbf{A} - E[\mathbf{A}] + (E[\mathbf{B}] - \mathbf{B})\mathbf{G} & (\mathbf{B} - E[\mathbf{B}])\mathbf{G} + E[\mathbf{A}] - \mathbf{L}E[\mathbf{C}] \\ +\mathbf{L}(E[\mathbf{C}] - \mathbf{C}) & \end{array} \right]$$

$$\tilde{\mathbf{B}} = \left[\begin{array}{c|c} \mathbf{F} & \mathbf{0} \\ \hline \mathbf{0} & -\mathbf{L}\mathbf{E} \end{array} \right]$$

where $\hat{\mathbf{x}}$ is the estimation of \mathbf{x} , $\tilde{\mathbf{x}} = [\mathbf{x}^T, \mathbf{g}^T]^T$ is the augmented state vector, $\mathbf{g} = \mathbf{x} - \hat{\mathbf{x}}$ is the estimation error, $\tilde{\mathbf{C}} = [\mathbf{C}^T | \mathbf{0}^T]^T$ and $\tilde{\mathbf{E}} = [\mathbf{0}^T | \mathbf{E}^T]^T$. The vector \mathbf{k} is formed by the feedback gain \mathbf{G} and the observer gain \mathbf{L} . Notice that the separation principle holds, i.e., $\tilde{\mathbf{A}}$ is upper triangular, if the deterministic plant used to generate the observer matches the dynamic system exactly. However, in general, the Separation Principle does not hold due to uncertainty in the plant model. In addition, the random closed-loop poles do not occur at the locations selected for the full-state feedback, i.e. poles of the $\tilde{\mathbf{A}}_{1,1}$ subsystem, nor at the locations for the full-order observer, i.e. poles of the $\tilde{\mathbf{A}}_{2,2}$ subsystem.

In this paper we propose a methodology for robust control design for systems with probabilistic uncertainty. Some of the major differences between the proposed strategy and conventional robust control methods are: (i) unnecessary conservatism is eliminated since there is not need for convex or bounded supports, (ii) the most likely plants are favored during synthesis allowing for probabilistic robust optimality, (iii) the tradeoff between robust stability and robust performance can be explored, (iv) the uncertainty set is closely related to parameters with clear physical meaning, and (v) compensators with improved robust characteristics for a given control structure, e.g., PID, can be designed.

3 Reliability-Based Metrics

The propagation of a fixed set of parameters of the plant through conventional control analysis tools leads to set of scalar quantities, e.g., closed loop poles, and a set of functions, e.g., step responses and Bode plots. The propagation of probabilistic uncertainty through the same tools leads to random variables, e.g., random closed-loop poles, and random processes, e.g., the step responses become random processes parameterized by time and the Bode plots become random processes parameterized by frequency. In this section we first introduce reliability metrics for random variables and processes. Such metrics will be used to quantify the violation of the design requirements. Specific realizations corresponding to stability, time and frequency requirements are then provided. In general, we will use x and $x(h)$ to denote a random variable and a random process dependent on \mathbf{p} through the plant model. For the random process $x(h)$, h refers to an arbitrary variable such as time or frequency.

3.1 Random Variables

We first introduce the concept of probability of failure. Let $x(\mathbf{p})$ be the random variable of interest. Let $x > \underline{x}$ be a design requirement. The event $x \leq \underline{x}$ will be referred to as failure. The corresponding failure set is given by $\mathcal{F} = \{x \mid x \in (-\infty, \underline{x}]\}$, where the failure boundary \underline{x} is a deterministic quantity prescribed in advance. The admissible domain, namely $\mathcal{A} = \{x \mid x \in (\underline{x}, \infty)\}$, is the complement of the failure domain. The same type of discrimination can be done in the parameter space \mathbf{p} by using $x(\mathbf{p})$. The function $g(\mathbf{p}, \underline{x}) = x(\mathbf{p}) - \underline{x}$, called the *limit state function*, divides the parameter space in two parts, the domain leading to \mathcal{A} , i.e., $g(\mathbf{p}, \underline{x}) > 0$, and the domain leading to \mathcal{F} , i.e., $g(\mathbf{p}, \underline{x}) \leq 0$. Hence, \mathcal{F} results from mapping the set $\{\mathbf{p} \in \Delta_{\mathbf{p}} \mid g(\mathbf{p}, \underline{x}) \leq 0\}$ through $x(\mathbf{p})$. In this case, the probability of failure P_f is given by

$$P_f = \text{P}[x \leq \underline{x}] = \int_{\xi \leq \underline{x}} f_x(\xi) d\xi = \int_{g \leq 0} f_{\mathbf{p}}(\mathbf{p}) d\mathbf{p} \quad (6)$$

Similar expressions can be derived if the design requirement is $x < \bar{x}$. These expressions describe reliability metrics for the random variable x when a single constraint is present, i.e., $x > \underline{x}$ or $x < \bar{x}$. A reliability metric for the random variable x having

both constraints can be easily formed

$$r_x(\underline{x}, \bar{x}) \triangleq r_x(\underline{x}) + \bar{r}_x(\bar{x}) \quad (7)$$

where

$$r_x(\underline{x}) \triangleq \text{P}[x \leq \underline{x}] = F_x(\underline{x}) \quad (8)$$

$$\bar{r}_x(\bar{x}) \triangleq \text{P}[x > \bar{x}] = 1 - F_x(\bar{x}) \quad (9)$$

Notice that $r_x(\underline{x})$ is equivalent to P_f in Equation (6). We will refer to \underline{x} and \bar{x} as the boundaries of the failure domain $\mathcal{F} = \{x \mid x \in (-\infty, \underline{x}] \cup (\bar{x}, \infty)\}$. Notice that the under-bar and the over-bar refer to the bound from below and the bound from above of the admissible domain $\mathcal{A} = \{x \mid x \in [\underline{x}, \bar{x}]\}$. This convention will be used for the remainder of the paper. Notice that the mapping of the corresponding limit state function through $x(\mathbf{p})$ leads to the failure boundary(s). Hence, there is a direct correspondence between \mathcal{F} and g . A sketch with relevant information is provided in Figure 1.

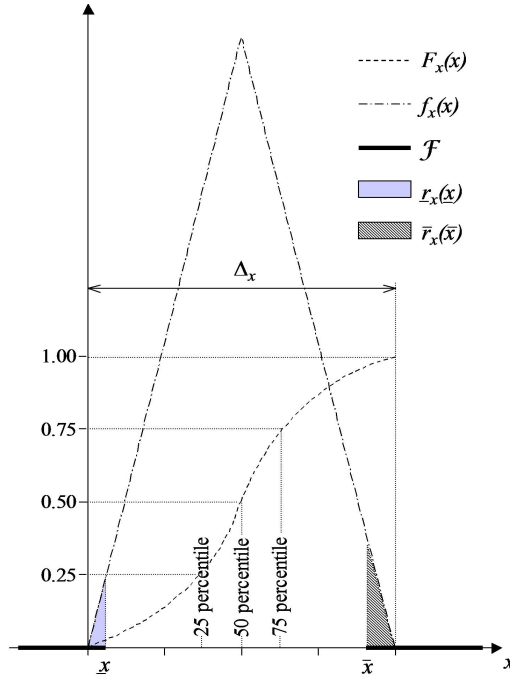


Figure 1. Sketch of the reliability metric for x .

3.2 Random Processes

The random process $x(h)$ can be considered as the parameterization of the random variable x by the deterministic variable h . In this paper $h \in [0, \infty]$ is assumed. The random process $x(h)$ is specified by the set of CDFs [15] $F_{x(h)}(x, h)$. For instance,

the system output $y(t)$ is prescribed by $F_{y(t)}(y, t)$. The evaluation of the process at a particular h value, say h_i , leads to the random variable $x(h_i)$ whose CDF is given by $F_x(x) = F_{x(h)}(x, h_i)$. In general, the support and the percentiles of $x(h)$ vary with h .

Let $x(h) > \underline{x}(h)$ for $h \in [h_1, h_2]$ and $x(h) \leq \bar{x}(h)$ for $h \in [h_3, h_4]$ be design requirements for the random process $x(h)$. In this paper, reliability metrics for processes are formulated by extending the ideas presented above. This is attained by integrating the reliability metric in Equation (7) for the random variable $x(h_i)$ in the h -interval of interest. In this context, a reliability metric for $x(h)$ is cast as

$$r_{x(h)}(\underline{x}(\cdot), \bar{x}(\cdot)) \triangleq r_{\underline{x}(\cdot)}(\underline{x}(\cdot)) + \bar{r}_{\bar{x}(h)}(\bar{x}(h)) \quad (10)$$

where

$$r_{\underline{x}(h)}(\underline{x}(\cdot)) \triangleq \frac{1}{h_2 - h_1} \int_{h_1}^{h_2} \mathbb{P}[x(h) \leq \underline{x}(h)] dh = \frac{1}{h_2 - h_1} \int_{h_1}^{h_2} F_{x(h)}(\underline{x}(h), h) dh \quad (11)$$

$$\bar{r}_{\bar{x}(h)}(\bar{x}(\cdot)) \triangleq \frac{1}{h_4 - h_3} \int_{h_3}^{h_4} \mathbb{P}[x(h) > \bar{x}(h)] dh = \frac{1}{h_4 - h_3} \int_{h_3}^{h_4} 1 - F_{x(h)}(\bar{x}(h), h) dh \quad (12)$$

are the costs of violating the lower and upper constraints respectively. These constraints, namely $\underline{x}(h)$ and $\bar{x}(h)$, will also be referred to as failure boundary functions. Notice that the failure domain

$$\mathcal{F} = \left\{ \bigcup_{h \in [h_1, h_2]} \{(x, h) | x \leq \underline{x}(h)\} \right\} \cup \left\{ \bigcup_{h \in [h_3, h_4]} \{(x, h) | x \geq \bar{x}(h)\} \right\}$$

is delimited by the failure boundaries. Observe that Equation (10) is a natural extension of Equation (7). A sketch with some of the pertinent metrics is provided in Figure 2. On the top plot, the 1, 25, 75 and 99 percentiles² are shown along with the failure boundaries $\underline{x}(h)$ and $\bar{x}(h)$ which, for this example, are linear. On the bottom plot, the integrands of Equations (11-12) corresponding to the configuration in the top plot are shown. Notice that if the process is contained within the set \mathcal{A} , the reliability metric $r_{x(h)}$ is zero, meaning that the inequality constraints are satisfied for all parameter values in $\Delta_{\mathbf{p}}$.

3.3 Realizations

3.3.1 Robust Stability

A LTI system is *robustly stable* if all its poles are in the open left half of the complex plane for all possible values of the random parameters. A reliability assessment of stability is given by

$$\mathbb{P} \left[\bigcup_{i=1}^v (\Re[s_i] > 0) \right] = \epsilon$$

²Recall that the m percentile, given by the x values satisfying $F_{x(h)}(x, h) = m/100$, defines a line under which $m\%$ of the probability lies. These lines allow us to visualize the h dependence of the PDF.

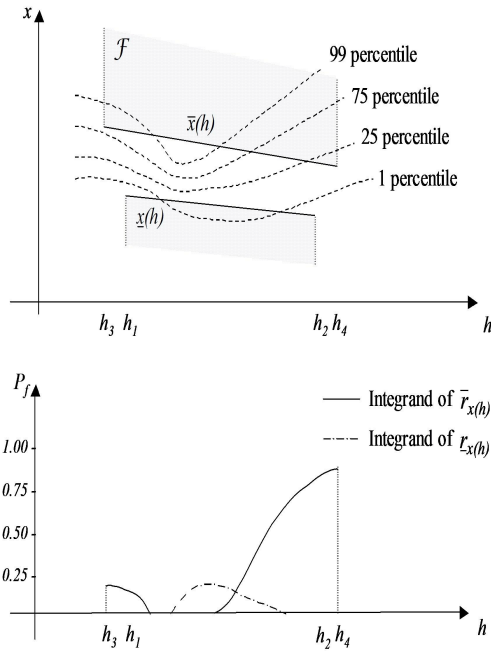


Figure 2. Sketch of the reliability metric for $x(h)$.

where s_i with $i = 1, 2, \dots, v$ is a random pole, $\Re[\cdot]$ is the real part operator and ϵ is the resulting probability of instability. Robust stability is attained if $\epsilon = 0$. Stability can also be cast via

$$\lambda \triangleq \max\{\Re[s_1], \Re[s_2], \dots, \Re[s_v]\} \quad (13)$$

In terms of λ , the probability of instability is given by $\bar{r}_\lambda(0)$. Robust stability is attained if $\bar{r}_\lambda(0) = 0$. Several comments are now pertinent. Reaching robust stability may not be feasible for the given support $\Delta_{\mathbf{p}}$ (even though it is bounded) and the assumed control structure $K(\mathbf{k})$. Notice also that the acceptance of a small non-zero probability of instability could be desirable from the performance point of view. For instance, by allowing the right low-probability tail of $f_\lambda(\lambda)$ to lie on the closed right half of the complex plane, a significant enhancement in the performance of the plants associated with the high probability portions of the PDF can be attained. Rather than advocating for the acceptance of the risk that this practice implies, we would like to highlight that the tradeoff between robustness and performance can be studied by allowing small positive values of ϵ .

3.3.2 Time-Domain

Quite frequently, performance requirements are prescribed in terms of time-domain specifications. The propagation of $f_{\mathbf{p}}(\mathbf{p})$ through the system dynamics leads to random processes for the time responses. Denote by $x(t)$ an arbitrary random process with CDF $F_{x(t)}(x, t)$. Such process is parameterized by \mathbf{p} , time t and the

compensator design variable \mathbf{k} . The dependence of $x(t)$ on \mathbf{k} has been omitted for the sake of simplifying the notation. Reliability metrics for relevant processes can be cast using Equation (10). For instance, while settling time and overshoot requirements for a Single Input Single Output (SISO) system, i.e., $\mathbf{u} \in \mathbb{R}$ and $\mathbf{y} \in \mathbb{R}$, are integrated using $r_{\mathbf{y}(t)}(\underline{\mathbf{y}}(t), \bar{\mathbf{y}}(t))$, the control saturation requirement $|\mathbf{u}| < u_{max}$ leads to $r_{\mathbf{u}(t)}(-u_{max}, u_{max})$.

A reliability metric for assessing the effects of noise on the uncertain plant is formulated next. The state covariance matrix, defined as $\mathbf{Q}(t) = \mathbb{E}[\tilde{\mathbf{x}}(t)\tilde{\mathbf{x}}^T(t)]$, is given by the solution to the Lyapunov equation

$$\dot{\mathbf{Q}} = \tilde{\mathbf{A}}\mathbf{Q} + \mathbf{Q}\tilde{\mathbf{A}}^T + \tilde{\mathbf{B}}\tilde{\mathbf{S}}\tilde{\mathbf{B}}^T \quad (14)$$

subject to $\mathbf{Q}(0) = \mathbf{Q}_0$. The output covariance, defined as $\mathbb{E}[\tilde{\mathbf{y}}(t)\tilde{\mathbf{y}}^T(t)]$, reaches the steady-state Root Mean Square (RMS) value

$$\tilde{\mathbf{y}}_{rms} = \lim_{t \rightarrow \infty} \text{diag} \left[\tilde{\mathbf{C}}\mathbf{Q}(t)\tilde{\mathbf{C}}^T \right]^{1/2} \quad (15)$$

Notice that uncertainty in \mathbf{p} makes $\tilde{\mathbf{y}}_{rms}$ a random vector. For instance, a reliability metric that penalizes the violation $\tilde{\mathbf{y}}_{rms} > \bar{\mathbf{y}}_{rms}$ where $\tilde{\mathbf{y}}_{rms} \in \mathbb{R}$ is given by $\bar{r}_{\tilde{\mathbf{y}}_{rms}}(\bar{\mathbf{y}}_{rms})$.

3.3.3 Frequency-Domain

The propagation of $f_{\mathbf{p}}(\mathbf{p})$ through the system dynamics onto the frequency domain leads to random processes of the form $x(\omega)$, whose probabilistic behavior at each ω is specified by $F_{x(\omega)}(x, \omega)$. Here, $x(\omega)$ is any real frequency dependent metric of the feedback loop, e.g. Bode magnitude. This random process is parameterized by \mathbf{p} , frequency ω and the compensator design variable \mathbf{k} . A reliability metric for $x(\omega)$ is $r_{x(\omega)}(\bar{x}(\omega), \underline{x}(\omega))$. For instance, conventional control requirements [16] for disturbance rejection, noise attenuation and reference tracking can be cast in terms of the loop transfer function $q(\omega) \triangleq |GK|$. Low frequency requirements can be cast using $r_{q(\omega)}(\underline{q}(\omega))$ with $\underline{q}(\omega) \equiv 1$ and high frequency requirements with $\bar{r}_{q(\omega)}(\bar{q}(\omega))$ for which $\bar{q}(\omega)$ has a proper roll off, each over a suitable range of frequencies.

3.4 Reliability Bounds

The following lemma, based on the Tchebyshev inequality, sets bounds for the reliability metrics introduced above in terms of the first and second order moments.

Lemma 1. *Let $\mathbb{E}[\cdot]$ and $\mathbb{V}[\cdot]$ denote the expected value and variance operators.*

$$r_x(\underline{x}) \leq \frac{\mathbb{V}[x]}{(\mathbb{E}[x] - \underline{x})^2} \text{ if } \underline{x} < \mathbb{E}[x] \quad (16)$$

$$\bar{r}_x(\bar{x}) \leq \frac{\mathbb{V}[x]}{(\bar{x} - \mathbb{E}[x])^2} \text{ if } \bar{x} > \mathbb{E}[x] \quad (17)$$

Proof. If $\epsilon > 0$

$$V[x] \geq \int_{|\xi - E[x]| > \epsilon} (\xi - E[x])^2 f_x(\xi) d\xi \geq \epsilon^2 P[|x - E[x]| > \epsilon] \geq \epsilon^2 P[x < E[x] - \epsilon]$$

We obtain Equation (16) using $\underline{x} = E[x] - \epsilon$. Equation (17) is derived following the same lines. \square

Notice that these bounds apply to any PDF of x . Since the bounds are solely dependent on the first two order moments they can be estimated more accurately than exact failure probabilities. Notice however that the use of bounds instead of reliability metrics introduces conservatism into the solution. A metric, based on these bounds, is defined as

$$b_x(\underline{x}, \bar{x}) \triangleq \underline{b}_x(\underline{x}) + \bar{b}_x(\bar{x}) \quad (18)$$

where

$$\underline{b}_x(\underline{x}) \triangleq \begin{cases} \frac{V[x]}{(E[x] - \underline{x})^2} & \text{if } \underline{x} < E[x] \\ \infty & \text{otherwise} \end{cases} \quad (19)$$

$$\bar{b}_x(\bar{x}) \triangleq \begin{cases} \frac{V[x]}{(\bar{x} - E[x])^2} & \text{if } \bar{x} > E[x] \\ \infty & \text{otherwise} \end{cases} \quad (20)$$

As before, the under-bar and over-bar on b refer to the way in which the failure event is defined. Notice that $r_x \leq b_x$, $\underline{r}_x(\underline{x}) \leq \underline{b}_x(\underline{x})$ and $\bar{r}_x(\bar{x}) \leq \bar{b}_x(\bar{x})$. The same idea, extended to random processes, leads to

$$b_{x(h)}(\bar{x}(\cdot), \underline{x}(\cdot)) \triangleq \underline{b}_{x(h)}(\underline{x}(\cdot)) + \bar{b}_{x(h)}(\bar{x}(\cdot)) \quad (21)$$

where

$$\underline{b}_{x(h)}(\underline{x}(\cdot)) \triangleq \begin{cases} \frac{1}{h_2 - h_1} \int_{h_1}^{h_2} \underline{b}_x(\underline{x}(h)) dh & \text{if } \underline{x}(h) < E[x(h)] \forall h \in [h_1, h_2] \\ \infty & \text{otherwise} \end{cases} \quad (22)$$

$$\bar{b}_{x(h)}(\bar{x}(\cdot)) \triangleq \begin{cases} \frac{1}{h_4 - h_3} \int_{h_3}^{h_4} \bar{b}_x(\bar{x}(h)) dh & \text{if } \bar{x}(h) > E[x(h)] \forall h \in [h_3, h_4] \\ \infty & \text{otherwise} \end{cases} \quad (23)$$

As before, $r_{x(h)} \leq b_{x(h)}$, $\underline{r}_{x(h)}(\underline{x}(\cdot)) \leq \underline{b}_{x(h)}(\underline{x}(\cdot))$ and $\bar{r}_{x(h)}(\bar{x}(\cdot)) \leq \bar{b}_{x(h)}(\bar{x}(\cdot))$.

4 Robustness-Based Metrics

Some performance requirements might not be properly captured in a conventional reliability formulation since they focus on the bulk portion of the PDF. Throughout this paper the term *robustness* is used to describe the design characteristic that measures the performance degradation from an ideal deterministic behavior caused by uncertainty. Robustness metrics, that quantify such a characteristic, are presented next. For random variables, the index

$$\tau_x(\hat{x}) \triangleq \int_{\Delta_x} (\xi - \hat{x})^2 f_x(\xi) d\xi = V[x] + E[x](E[x] - 2\hat{x}) + \hat{x}^2 \quad (24)$$

is a measure of the concentration of $f_x(x)$ about the deterministic target value \hat{x} . In the ideal case when $f_x(x) = \delta(x - \hat{x})$, we obtain $\tau_x(\hat{x}) = 0$. For random processes, the index

$$\tau_{x(h)}(\hat{x}(\cdot)) \triangleq \frac{1}{h_6 - h_5} \int_{h_5}^{h_6} \tau_x(\hat{x}(h)) dh \quad (25)$$

is a measure of the concentration of the process $x(h)$ about the deterministic target function $\hat{x}(h)$ for $h \in [h_5, h_6]$. Notice that the evaluation of the above expressions only requires of the first two order moments of the process.

Robustness-based metrics parallel to the ones provided in Section 3.3 can easily be posed. For instance, if \mathbf{y}_{rms} is the RMS steady state value of an error signal, the index $\tau_{\mathbf{y}_{rms}}(0)$ quantifies the offset between the target behavior $\hat{\mathbf{y}}_{rms} = 0$ and the random variable \mathbf{y}_{rms} . Likewise, the metric $\tau_{\mathbf{u}(t)}(0)$ quantifies the offset between the random process $\mathbf{u}(t) \in \mathbb{R}$ and the target $\hat{\mathbf{u}} = 0$, for which no actuation is required.

5 Numerical Estimation

Methods used for the estimation of the reliability- and robustness-based metrics introduced above are presented herein. Historically, mathematical studies of reliability engineering systems have focused on approximation of “probability of failure.” Some of the techniques historically used for this approximation are particularly suited for estimating probabilities near zero, which is the range in which one hopes a probability of failure will lie. In this study, we will be concerned with estimating the probabilities of various random events. In this paper, events in a reliability framework might be referred to as “failure events” to be consistent with previous usage whether they actually represent a failure of some sort or not. The reader should also be aware that any estimation technique that works well for failure probabilities near zero also work well for events of probability near one after using the complementary event instead.

Only the estimation of statistics for x will be addressed since the same tools can be extended to processes. Such an extension is as follows. For the random process $x(h)$, create a uniform sample of e points h_1, h_2, \dots, h_e in the h -domain. We will refer to these samples as the e *h-samples*. Statistics for the resulting e random variables $x_i = x(h_i)$, $i = 1, 2 \dots e$ are then used to estimate the pertinent integrals, i.e., Equations (11), (12), (22), (23), and (25).

5.1 Hammersley-Sequence-Sampling (HSS)

HSS generates representative deterministic samples of $f_{\mathbf{p}}(\mathbf{p})$. The error of approximating an integral by a finite number of samples of the integrand, depends on the uniformity of the points used to generate the samples rather than on their randomness. This fact has motivated the development of deterministic sampling techniques such as HSS. While conventional Monte Carlo Sampling (MCS) is based on the generation of random points on the unit hypercube, HSS is based on the generation of an evenly distributed set of points. The n Hammersley samples are generated by

transforming the n Hammersley points \mathbf{m}_i with $i = 1, 2, \dots, n$ through the inverse CDF of the uncertain parameter

$$\mathbf{p}_i = F_{\mathbf{p}}^{-1}(\mathbf{m}_i) \quad (26)$$

The Hammersley points [17] are generated as follows. Let $R > 1$ be an integer. The integer i expressed in radix- R notation is given by

$$i = \sum_{j=0}^v i_j R^j$$

where $v = \text{floor}\{\log_R i\}$ and i_j is an integer between 0 and $R - 1$ for each $j = 0, 1, \dots, v$. The inverse radix number of i , namely $\phi_R(i)$, is given by

$$\phi_R(i) = \sum_{j=0}^v \frac{i_j}{R^{j+1}}$$

The Hammersley points in a k -dimensional unit hypercube are given by the sequence

$$\mathbf{m}_i = \mathbf{1} - [i/n, \phi_{R_1}(i), \phi_{R_2}(i), \dots, \phi_{R_{k-1}}(i)]^T \quad (27)$$

where $i = 1, 2, \dots, n$ and R_j is the j th prime number.

HSS requires far fewer samples [18] than MCS [5–7, 14] for a given confidence level. Improvements by a factor of three to one hundred in the convergence rate of the estimated first two order moments have been reported [19]. Another way to observe the advantages of HSS over MCS is to note that, for the same sample size, the HSS sample is more representative of the random distribution than the MCS sample. Figure 3 shows a comparison between HSS and MCS. At the top, $n = 200$ points on the unit hypercube are shown. At the bottom, the corresponding samples for $f_{\mathbf{p}}(\mathbf{p}) = f_a(a)f_b(b)$, where $f_a(a) = N(0, 1)$ and $f_b(b) = B(3, 2)$ with $\Delta_b = [0, 1]$ are displayed. Here, N and B denote a Normal and a Beta distribution. Substantial differences in the uniformity of the points and in the clustering of the samples are observed. In addition, the results of calculations based on HSS samples are not random. On the other hand, numerical experiments performed using MCS show variability due to such factors as different implements of random number generators and different random seeds resulting in the generation of completely different sample sets. The discrepancy between different MCS experiments is more pronounced with small sample size, and could be reduced, but not completely eliminated, by an increase, possibly substantial, in the sample size. Therefore, HSS not only leads to more accurate estimations than MCS for a given number of samples but also eliminates the randomness from the estimation.

5.2 Mean and Variances

The reliability bounds and the robustness metrics introduced above depend exclusively on means and variances. In this paper, Sampling and the First and Second Moment Second Order approximations are used for their estimation. These methods are briefly introduced next.

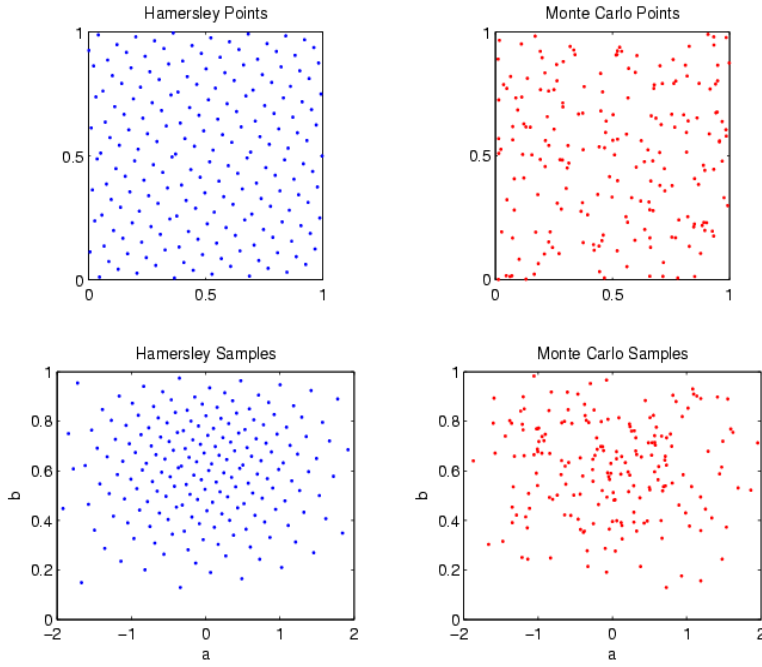


Figure 3. Points and samples via MCS and HSS.

5.2.1 Sampling

Unbiased estimators for the mean and variance of the random variable x are

$$E[x] \approx \frac{1}{n} \sum_{i=1}^n x_i \quad (28)$$

$$V[x] \approx \frac{1}{n-1} \sum_{i=1}^n (x_i - E[x])^2 \quad (29)$$

where $x_i = x(\mathbf{p}_i)$ is the i th sample. The \mathbf{p}_i sample of $f_{\mathbf{p}}(\mathbf{p})$ can be generated by any sampling technique.

5.2.2 First and Second Moments of a Second Order Taylor approximation (FSMSO)

These approximations result from calculating the first and second moment of a second order Taylor expansion of $x(\mathbf{p})$ about $E[\mathbf{p}]$. Let $\mathbf{p} \in \mathbb{R}^m$, and \mathbf{p}_i be the i th

component of \mathbf{p} . For an uncorrelated $f_{\mathbf{p}}(\mathbf{p})$, the resulting approximations are

$$E[x] \approx x + \frac{1}{2} \sum_{i=1}^m \frac{\partial^2 x}{\partial \mathbf{p}^{(i)2}} V[\mathbf{p}^{(i)}] \quad (30)$$

$$\begin{aligned} V[x] \approx & \sum_{i=1}^m \left[\left(\frac{\partial x}{\partial \mathbf{p}^{(i)}} \right)^2 V[\mathbf{p}^{(i)}] + \left(\frac{\partial x}{\partial \mathbf{p}^{(i)}} \right) \left(\frac{\partial^2 x}{\partial \mathbf{p}^{(i)2}} \right) T[\mathbf{p}^{(i)}] \right] \\ & + \sum_{i=1}^m \frac{1}{4} \left(\frac{\partial^2 x}{\partial \mathbf{p}^{(i)2}} \right)^2 (F[\mathbf{p}^{(i)}] - V[\mathbf{p}^{(i)}]^2) \\ & + \sum_{i=1}^m \sum_{j \neq i}^m \frac{1}{2} \left(\frac{\partial^2 x}{\partial \mathbf{p}^{(i)} \partial \mathbf{p}^{(j)}} \right)^2 V[\mathbf{p}^{(i)}] V[\mathbf{p}^{(j)}] \end{aligned} \quad (31)$$

where the functions and derivatives are evaluated at $E[\mathbf{p}]$, $T[\cdot]$ is the third central moment operator and $F[\cdot]$ is the fourth.

5.3 Failure probabilities

In general, reliability metrics cannot be evaluated exactly since they involve the evaluation of complicated integrals, usually multi-dimensional, over complex domains. The estimation of failure probabilities, which are basic components of the reliability metrics, can be done using sampling or asymptotic approximations. They are briefly introduced next.

5.3.1 Sampling

The estimation of failure probabilities via sampling is given by

$$P_f \approx \sum_{i=1}^n \frac{\mathcal{I}(x_i \in \mathcal{F})}{n} \quad (32)$$

where $\mathcal{I}(\cdot)$ is a binary indicator function that gives one if its argument is true and zero otherwise. MCS and HSS can be used to generate the required samples x_1, x_2, \dots, x_n .

5.3.2 First-Order-Reliability-Method (FORM)

FORM [12] uses an asymptotic approximation for the estimation of failure probabilities. In the process, \mathbf{p} is transformed into the standard normal uncorrelated space \mathbf{q} . If $\mathbf{p} = \mathbf{T}(\mathbf{q}) = F_{\mathbf{p}}^{-1}(F_{\mathbf{q}}(\mathbf{q}))$, Equation (6) is equivalent to

$$P_f = \int_{g(\mathbf{T}(\mathbf{q})) \leq 0} f_{\mathbf{q}}(\mathbf{q}) d\mathbf{q}$$

FORM approximates the domain $g(\mathbf{T}(\mathbf{q})) \leq 0$, by a half-space fitted to the true domain at the point of maximum probability density. This approximation leads to

$$P_f \approx \Phi(-\|\mathbf{q}^*\|) \quad (33)$$

where \mathbf{q}^* , called the *Most Probable Point* (MPP) of failure, is given by the solution to the constrained optimization problem $\mathbf{q}^* = \operatorname{argmin} \{\|\mathbf{q}\| : g(\mathbf{T}(\mathbf{q})) = 0\}$. In this expression, Φ refers to the CDF of a standard normal random variable. Notice that the rotational symmetry of $f_{\mathbf{q}}(\mathbf{q})$ leads to the one-dimensional approximation in Equation (33). When a point satisfying $g(\mathbf{T}(\mathbf{q})) = 0$ does not exist, the MPP does not exist and the probability of failure is zero or one. Even though FORM is extensively used in structural engineering, its application to controls has been limited to stability analysis [11]. Non-smooth limit state functions happen in examples of interest. For instance, when the value of λ , the maximum real part of the eigenvalues, is equal to the real part of more than one of the eigenvalues (counting multiplicity). This consideration shall be taken into account when setting the algorithm to search for the MPP. Besides, if the MPP falls at a derivative discontinuity on the limit state surface, the approximation given by Equation (33) is not as good as first order.

5.3.3 Hybrid Approach

Sampling based techniques can readily be used to estimate probabilities of failure using Equation (32). However, high computational demands in the evaluation of $x_i = x(\mathbf{p}_i)$ can preclude their practicality especially when $P_f \approx 0$ (or $P_f \approx 1$). Examples of this can be easily found³. On the other hand, methods based on asymptotic approximations, such as FORM, provide good approximations when P_f is small. This is clear since for large values of \mathbf{q} , $f_{\mathbf{q}}(\mathbf{q})$ decreases exponentially in $\|\mathbf{q}\|^2$, so if \mathbf{q}^* is large enough, most of the failure probability comes from the part of the failure event in the immediate neighborhood of \mathbf{q}^* . On the other hand, for failure probabilities away from zero and one, the slow decrease in $F_{\mathbf{q}}(\mathbf{q})$ near the MPP and the geometrical difference between the true limit state function and its linear approximation contribute a bigger error to the FORM approximation.

In this paper, a hybrid approach which combines HSS and FORM is used to estimate probabilities of failure. In order to identify the numerical tool that best suits the task at hand, a coarse and computationally-efficient estimation of P_f is first generated using HSS. Such estimation is then compared with a reference, namely the *reference failure probability* P_{ref} , a user-defined value set in advance. The comparison between the coarse estimate and P_{ref} is used to determine which of FORM or HSS will be used to generate a new estimation, presumably more accurate. Assume that two sets of Hammersley samples of $f_{\mathbf{p}}(\mathbf{p})$ are available. One set has n_1 samples and the other one has n_2 samples, where $n_2 \gg n_1$. For a given failure domain \mathcal{F} and a user defined reference failure probability P_{ref} , proceed as follows

1. A_1 Assessment: estimate the P_f using Equation (32) and the set of n_1 samples.
2. A_2 Assessment: recalculate P_f as follows. If the estimated value is greater than P_{ref} use Equation (32) with the set of n_2 samples. If the estimated value is less than P_{ref} use FORM.

³Wang and Stengel [6, 7] make the approach computationally viable by using a single random variable to model 28 uncertain parameters. The same authors [14] require 25000 samples to determine a sufficiently small 95% confidence interval.

The refinement performed in A_2 might not always be necessary. Situations in which this is the case are as follows. Since reliability metrics for random processes are heavily dependent on the larger values of the probabilities of failure that compose them, (see the bottom plot of Figure 2), refining the estimation of the small failure probabilities is inconsequential. Furthermore, if the reliability metrics are used to calculate the cost function of an optimization problem, more accurate estimations are not needed when the assessment resulting from using the coarse estimate of Step 1 indicates a poor design, e.g. $\bar{r}_\lambda(0) \gg 0$.

6 Control Synthesis

6.1 Reliability-based

The formulation of the control design problem from a reliability perspective is as follows. For a given plant model, compensator structure, uncertainty model and a set of design requirements prescribed via inequality constraints; one would like to find the compensator parameters for which the resulting probability of violating the design requirements is minimized. Notice that this refers to the excursion of the outcomes into the failure domains.

6.1.1 Robustness Considerations

The reliability metrics in Equations (7-10) are usually applied using a fixed failure set \mathcal{F} . In this form, a reliability analysis cannot assess the system's performance in the regions where the design requirements are satisfied, i.e., the intersection of the admissible domains associated with all the design requirements. Since the portion of the random outcome lying in the admissible domain \mathcal{A} might end up being substantially larger than the portion lying in the failure domain \mathcal{F} , a reliability-based approach with fixed failure boundaries does not have control over the bulk portion of the PDF, which is the portion that dictates the most likely performance.

We now introduce the concept of a shapable failure set \mathcal{F} with an example. Let $x(\mathbf{k})$ be the stationary RMS value of an error signal. One would like to find \mathbf{k} such that x is as close as possible to zero. Uncertainty in the plant makes x a random variable. Let \bar{x} be the failure boundary associated with the design requirement $x < \bar{x}$, i.e., a fixed failure set is $\mathcal{F} = \{x \mid x \in [\bar{x}, \infty)\}$. The minimization of $\bar{r}_x(\bar{x})$ leads to reliability optimal compensators. Suppose there exist multiple designs leading to $\bar{r}_x(\bar{x}) = 0$. These designs however differ in how well the resulting PDF of x spreads over the admissible domain $\mathcal{A} = \{x \mid x \in [0, \bar{x})\}$. The concentration of $f_x(x)$ about zero is an indicator of the robust performance. Say, \mathbf{k}_1 leads to $\bar{r}_x(\bar{x}/2) = 0$ which implies that $\bar{r}_x(\bar{x}) = 0$ while \mathbf{k}_2 leads to $\bar{r}_x(\bar{x}) = 0$ but $\bar{r}_x(\bar{x}/2) > 0$. Since neither of these two designs violate the design requirement $x > \bar{x}$, a reliability analysis cannot establish that the compensator with parameters \mathbf{k}_1 has a better robust performance than the one which uses \mathbf{k}_2 . By minimizing the reliability metrics and simultaneously shrinking the admissible domain, the uncertain system performance can be concentrated in a more desirable region. This is attained by parameterizing the failure boundaries of \mathcal{F} as well as a penalizing function γ_x with

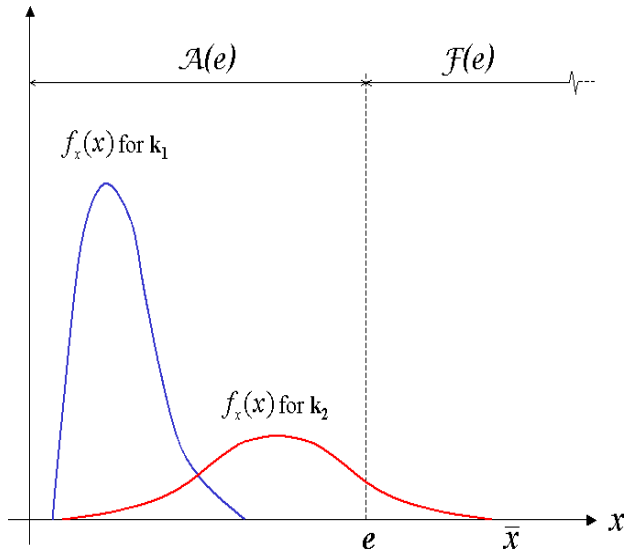


Figure 4. Robust performance concepts and shapable failure domains

an additional design variable, namely \mathbf{e} . The basic idea is to solve an optimization problem for the design variable $\mathbf{d} = [\mathbf{k}, \mathbf{e}]$ such that a twofold objective is pursued: a reliability metric is minimized while the size of \mathcal{A} is reduced. This implies that the failure and the admissible domains are now dependent on \mathbf{e} , i.e., $\mathcal{A}(\mathbf{e})$ and $\mathcal{F}(\mathbf{e})$. For the RMS example above, the minimization of $J = \bar{r}_x(\mathbf{e}) + \gamma_x$ where $\gamma_x = \mathbf{e}$, $\mathbf{d} = [\mathbf{k}, \mathbf{e}]$ and $\mathbf{e} \in [0, \bar{x}]$, leads to the desired solution. This setting implies $\mathcal{F}(\mathbf{e}) = \{x \mid x \in [\mathbf{e}, \infty)\}$ and $\mathcal{A}(\mathbf{e}) = \{x \mid x \in [0, \mathbf{e}]\}$. See Figure 4. Notice that the value of J for \mathbf{k}_1 is less than the one for \mathbf{k}_2 if $\mathbf{e} \in [\bar{x}/2, \bar{x})$.

In general, we will refer to the *augmented reliability metric* as the sum of a reliability metric from Section 3 and the penalizing term introduced above. Augmented reliability metrics for the random variable x and the random process $x(h)$ take the form $r_x(\underline{x}(\mathbf{e}), \bar{x}(\mathbf{e})) + \gamma_x(\mathbf{e})$ and $r_{x(h)}(\underline{x}(h, \mathbf{e}), \bar{x}(h, \mathbf{e})) + \gamma_{x(h)}(\mathbf{e})$. The penalizing functions $\gamma_x(\mathbf{e})$ and $\gamma_{x(h)}(\mathbf{e})$ must be proportional to the size of the admissible domain $\mathcal{A}(\mathbf{e})$. In addition, they must be built such that the minimization of the augmented metric does not lead to unacceptable solutions, e.g., $r_x = 1$ and $\gamma_x = 0$. If $r_x < \epsilon$ is required, use a monotonically increasing function satisfying $\gamma \in [0, \epsilon]$. In the RMS example above, for which $x < \bar{x}$ is the design requirement, this is attained by minimizing an augmented reliability metric with $\gamma_x(\mathbf{e}) = \epsilon \mathbf{e} / \bar{x}$ for $\mathbf{e} \in [0, \bar{x}]$, $\underline{x}(\mathbf{e}) = 0$ and $\bar{x}(\mathbf{e}) = \mathbf{e}$.

6.2 Robustness-based

The formulation of the control design problem from a robustness perspective is as follows. For a given plant model, compensator structure and uncertainty model; one would like to find the compensator parameters for which the resulting random outcome is as concentrated as possible around a target deterministic behavior. While

the deterministic target for a random variable is a scalar, the target for a random process is a function, e.g., $\hat{u}(t) = 0$ is the target function for the control.

6.3 Multi-objective Optimization

In order to satisfy multiple design requirements, all the corresponding reliability metrics must be driven to zero. Since some of these objectives are conflicting, a compromise among them might be required. The technique to be used reduces the multi-objective problem into a single objective problem given by a weighted sum of the reliability metrics. The solution to this problem will converge to a Pareto optimal point, which is a design for which no improvement on a single objective can be attained without making another worse. For each set of weights, the optimization may converge to a different Pareto point. Other techniques, such as the goal attainment method could be used instead.

6.4 Synthesis Procedure

A step-by-step procedure for control synthesis is presented next.

1. Determine the plant model and the control structure. First principles and classical deterministic approaches to compensator design can be used. Identify the set of parameters that have a strong impact on the plant model. Use sensitivity information and engineering judgment to select the set of uncertain parameters \mathbf{p} . At this stage, the parametric plant model, i.e., $G(\mathbf{p})$, and the control structure, i.e., $K(\mathbf{k})$, must be fully determined.
2. Generate the probabilistic parameter model $f_{\mathbf{p}}(\mathbf{p})$. Use engineering judgment and experimental data if available.
3. Use Equation (26) to generate the sample sets of $f_{\mathbf{p}}(\mathbf{p})$ for both n_1 and n_2 .
4. Cast the design requirements, either reliability or robustness based, in terms of the metrics introduced above. Use Equations (7,10) for the reliability metrics and Equations (24,25) for the robustness metrics. Recall that while each reliability requirement requires setting a failure domain \mathcal{F} , each robustness requirement requires setting a target behavior. Use these metrics to compose the *cost vector* \mathbf{c} , which is the vector of objectives for multi-objective optimization. Recall that robustness considerations can be alternatively considered within a reliability formulation, as explained in Section 6.1.1.
5. Let \mathbf{d} be the design variable. For robustness-based metrics and reliability-based metrics with fixed failure domains, $\mathbf{d} = \mathbf{k}$. Reliability-metrics with shapable failure domains lead to $\mathbf{d} = [\mathbf{k}^T, \mathbf{e}^T]^T$. Build a penalizing function $\gamma(\mathbf{e})$ for these terms following the guidelines provided in Section 6.1.1. Update the components of the cost vector \mathbf{c} by adding the penalizing functions and parameterizing the failure boundaries.

6. Solve the single objective optimization problem

$$\mathbf{d}^* = \operatorname{argmin} \{ \mathbf{c}^T \mathbf{w} \} \quad (34)$$

where \mathbf{w} is composed of non-negative weights. Each cost function evaluation used in the search for the optimal design \mathbf{d}^* requires a probabilistic analysis. This analysis is done by calculating the metrics contained in \mathbf{c} . While the hybrid approach is used for estimating the reliability metrics, either HSS or FSMSO are used for the robustness metrics. This task requires forming the closed-loop Equations (4-5) and performing typical control studies such as finding closed loop poles, time responses and Bode plots.

During optimization, the following procedure is suggested in order to focus most of the computational effort toward the assessment of better designs. For a reliability metric, first perform the A_1 assessment of Section 5.3.3 for n_1 samples of \mathbf{p} and e_1 h-samples. This implies that only the first step of the hybrid approach is applied to all reliability metrics. If A_1 shows that \mathbf{d} is a good design, perform the refined assessment A_2 . A_2 is carried out by using n_2 samples of \mathbf{p} , e_2 h-samples and a user defined value for P_{ref} . The rationale of this was presented in Section 5.3.3. For a robustness metric or a reliability bound, HSS or FSMSO could be used. In the former case, a first assessment can be done with the parameters of A_1 and a second one with the parameters of A_2 . This two-fold analysis procedure is used in the examples.

The cost vector \mathbf{c} can be formed by combinations of reliability-based metrics, reliability bounds and/or robustness-based metrics. The corresponding implications are explored in the examples.

6.5 Optimization under Uncertainty

Let $J(\mathbf{p}, \mathbf{d}) = \mathbf{c}^T \mathbf{w}$ denote the cost function of the optimization problem. Due to the nature of the reliability metrics in \mathbf{c} , the cost function might not only have plateaus, i.e., there could exist a design \mathbf{d} and a non-zero perturbation δ such that $J(\mathbf{p}, \mathbf{d}) = J(\mathbf{p}, \mathbf{d} + \delta)$, but might also have a discontinuous gradient.

The use of sampling in the estimation of probabilities makes the cost function piecewise constant. Let $J_e(\mathbf{p}, \mathbf{d})$ be an estimation of the actual cost $J(\mathbf{p}, \mathbf{d})$. For any design \mathbf{d} and regardless of the number of samples, there always exists a perturbation δ such that $J_e(\mathbf{p}, \mathbf{d}) = J_e(\mathbf{p}, \mathbf{d} + \delta)$. This situation is aggravated, i.e., bigger perturbations can be found, when a smaller number of samples is used or when P_f is close to zero or one.

Mean and variances can be estimated via sampling or via FSMSO. Their estimation via sampling does not exhibit the numerical problems mentioned above. Among the sampling techniques, it was found that HSS suites very well the need for an accurate and efficient estimation [18]. Estimation via FSMSO is considerably faster than sampling but less accurate in general. This is so, since the Taylor expansion might become a poor approximation of the actual function when $f_{\mathbf{p}}(\mathbf{p})$ is not concentrated about $E[\mathbf{p}]$.

The nature of J_e must be taken into account when selecting a numerical method for optimization. In the examples to follow, the resulting non-convex piecewise constant optimization problem is first solved using *Genetic Algorithms* (GA) for a fixed number of generations. Since GA is based on a random search, the hybrid approach is particularly convenient. After the fixed number of generations is reached, the GA solution is refined using the *Nelder Mead Simplex* algorithm, which is a local non-gradient based search method.

7 Numerical Examples

The synthesis procedure of Section 6.4 is applied herein to two examples. A textbook satellite attitude control problem is considered first. Then, the active control of a flexible beam subject to disturbances is considered. The following parameter values are assumed in both problems. If $\mathbf{p} \in \mathbb{R}^m$, the coarse assessment A_1 is performed using $n_1 = 75m$ \mathbf{p} -samples and $e_1 = 90$ h -samples. For the finer assessment A_2 , $n_2 = 500m$ \mathbf{p} -samples, $e_2 = 180$ h -samples and $P_{ref} = 0.01$ are assumed. For the sake of comparison, the examples also present the analysis of deterministic versions of the problems for which $E[\mathbf{p}]$ is used as parameter. Such problems and their solutions will be referred to as the *nominal* ones.

7.1 Satellite Attitude Control

Accurate satellite pointing in the presence of large thermal gradients and mass losses for uncertain initial conditions is desired. A simple rotational model of two bodies connected with a flexible boom leads to

$$\begin{aligned} J_1 \ddot{\theta}_1 + b(\dot{\theta}_1 - \dot{\theta}_2) + k(\theta_1 - \theta_2) &= u \\ J_2 \ddot{\theta}_2 + b(\dot{\theta}_2 - \dot{\theta}_1) + k(\theta_2 - \theta_1) &= 0 \end{aligned}$$

where θ_1 and θ_2 are the deflection angles, J_1 and J_2 are moments of inertia, k is the equivalent stiffness, $b = a\sqrt{k/10}$ is the equivalent damping coefficient and u is the applied torque. The variable a is used to model the changes in damping caused by thermal variations. Assume that $J_2 = 0.1$ since mass losses only affect J_1 . The non-collocated sensor-actuator pair resulting from using $y = \theta_2$ leads to the SISO system

$$G(\mathbf{p}) = \frac{k + bs}{J_1 J_2 s^4 + b(J_1 + J_2)s^3 + (J_1 + J_2)ks^2} \quad (35)$$

Variations in the operating conditions and ignorance on the initial conditions are modeled using $\mathbf{p} = [J_1, a, k, \theta_{1,0}, \dot{\theta}_{1,0}, \theta_{2,0}, \dot{\theta}_{2,0}]^T$, where $\theta_{1,0} = \theta_1(0)$ and $\theta_{2,0} = \theta_2(0)$. The following output-feedback control structure is assumed

$$K(\mathbf{k}) = \frac{k_1 + k_2 s + k_3 s^2 + k_4 s^3}{k_5 + k_6 s + k_7 s^2 + k_8 s^3} \quad (36)$$

The joint PDF that describes the uncertainty in \mathbf{p} is given by the independent random variables listed in Table 1, where U and B refer to Uniform and Beta distributions.

Table 1. Uncertainty Model.

J_1	$\Delta_{J_1} = [0.8, 1]$	$f_{J_1}(J_1) = U(0.8, 1)$
a	$\Delta_a = [0.03, 0.2]$	$f_a(a) = B(0.3, 0.2)$
k	$\Delta_k = [0.09, 0.4]$	$f_k(k) = B(5, 5)$
$\theta_{1,0}$	$\Delta_{\theta_{1,0}} = [-\pi/2, \pi/2]$	$f_{\theta_{1,0}}(\theta_{1,0}) = B(5.2, 5.2)$
$\dot{\theta}_{1,0}$	$\Delta_{\dot{\theta}_{1,0}} = [-15, 15]$	$f_{\dot{\theta}_{1,0}}(\dot{\theta}_{1,0}) = B(2.5, 2.5)$
$\theta_{2,0}$	$\Delta_{\theta_{2,0}} = [-\pi/2, \pi/2]$	$f_{\theta_{2,0}}(\theta_{2,0}) = B(5.2, 5.2)$
$\dot{\theta}_{2,0}$	$\Delta_{\dot{\theta}_{2,0}} = [-15, 15]$	$f_{\dot{\theta}_{2,0}}(\dot{\theta}_{2,0}) = B(2.5, 2.5)$

7.1.1 Nominal Compensator

A baseline compensator for the nominal plant is designed by standard pole placement techniques such that large stability margins are attained. For fairness sake, the baseline compensator's gains were selected such that the resulting closed-loop system is robustly stable for the uncertainty model of Table 1. The resulting gains are $\mathbf{k}_1 = 10^6[0.0108, -0.3271, 0.1192, 0.0092, 1.8835, 2.1305, 2.2276, 0.9308]^T$. The analysis of the nominal compensator using $f_{\mathbf{p}}(\mathbf{p})$ indicates that the closed-loop system is robustly stable as intended, i.e. $\bar{r}_\lambda(0) = 0$, but the time responses are unsatisfactory. The CDF of λ as well as the time evolutions of the output and the control signals are shown in Figures 5-7. The sudden variation in the slope of the CDF of λ in Figure 5 is the result of a change in the closed-loop pole that determines λ . The considerable disparity between $\lambda(E[\mathbf{p}])$ and $E[\lambda(\mathbf{p})]$ shows that the nominal problem is not a meaningful representative of the probabilistic behavior. Figures 6 and 7 show the time evolution of the random signals by indicating the 1, 10, 20, 30, 40, 50, 60, 70, 80, 90 and 99 percentiles. In Figures 6 and 7, the percentiles and the nominal functions are shown. Dotted lines are used to indicate the failure boundaries introduced in the next section. It is interesting to see how the PDFs expand, e.g. Figure 7 at 2.5 and 8 seconds, and contract, e.g. Figure 7 at 4 and 16 seconds, in an oscillatory manner. This information can be used to determine the time periods when the effects of uncertainty are more noticeable.

7.1.2 Reliability-based compensator

Design requirements for a reliability formulation are as follows. Performance requirements on the closed-loop stability, settling time, over-shoot, control usage and on the magnitude of the loop transfer function lead to $\mathbf{c} = [\bar{r}_\lambda(\bar{\lambda}), r_{y(t)}(\underline{y}(t), \bar{y}(t)), r_{u(t)}(\underline{u}, \bar{u}), r_{q(\omega)}(\underline{q}(\omega)), \bar{r}_{q(\omega)}(\bar{q}(\omega))]^T$, where $q(\omega) = |GK|$ is the loop gain. The failure boundaries to be used are $\bar{\lambda} = 0$; $\underline{y}(t) = -1.25\mathcal{H}(t) + 2.2\mathcal{H}(t-70)$ for $t \in [0, 80]$, where \mathcal{H} is the Heaviside function; $\bar{y}(t) = 1.25\mathcal{H}(t) - 0.2\mathcal{H}(t-70)$ for $t \in [0, 80]$; $\underline{u}(t) = -0.5$ for $t \in [0, 25]$; $\bar{u}(t) = 0.5$ for $t \in [0, 25]$; $\underline{q}(\omega) = 0.75/\omega$ for $\omega \in [10^{-6}, 0.2]$ and $\bar{q}(\omega) = 1$

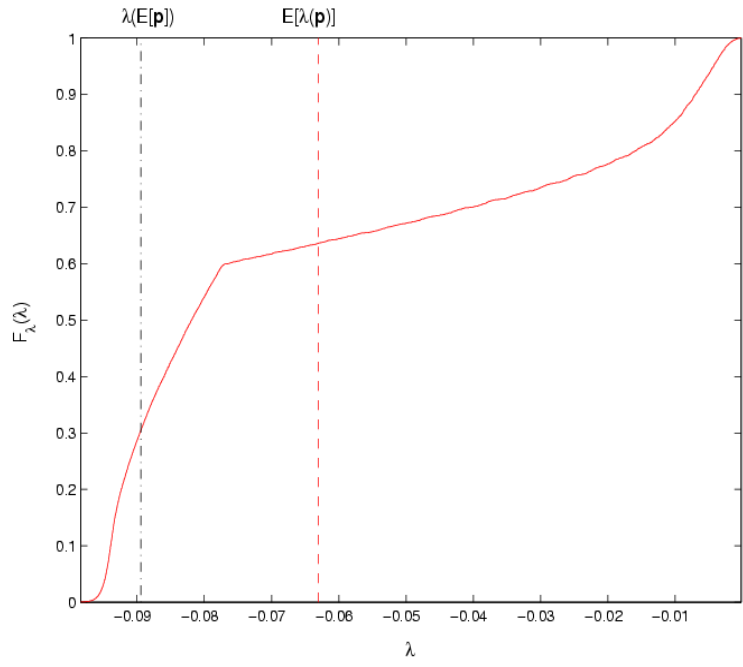


Figure 5. CDF of λ for the nominal compensator.

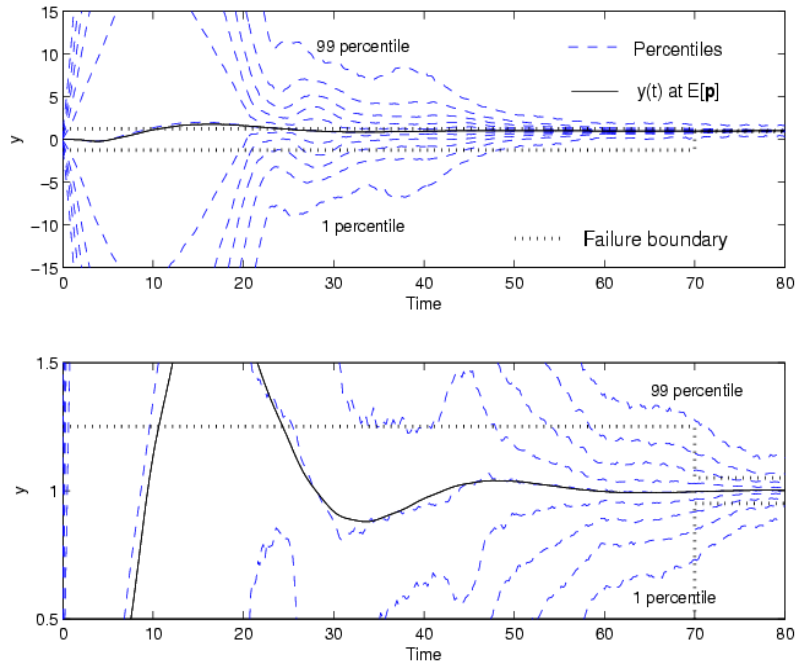


Figure 6. $y(t)$ for the nominal compensator. A zoom is shown below.

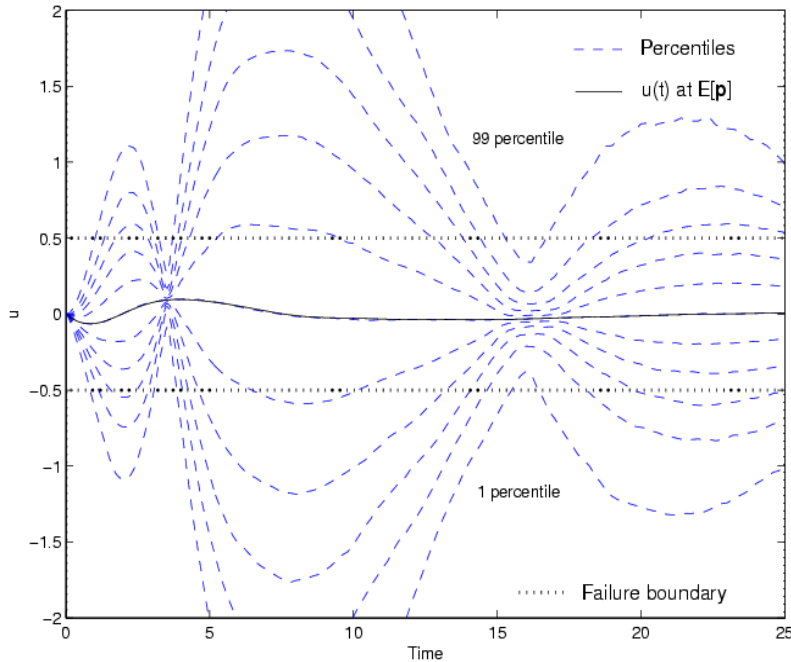


Figure 7. $u(t)$ for the nominal compensator.

for $\omega \in [1, 10^2]$.

The synthesis algorithm for a fixed set of failure boundaries leads to $\mathbf{k}_2 = 10^6[0.0405, 0.1267, 0.2422, 0.0320, 0.5244, 1.0057, 1.2263, 0.6560]^T$ and $\mathbf{c} = [3.13 \times 10^{-4}, 6.51 \times 10^{-4}, 0.0037, 6.65 \times 10^{-4}, 0]^T$ for which the weighting vector $\mathbf{w} = [500, 1, 1, 1, 1]^T$ was used. This weighting vector was selected in order to emphasize stability. A probabilistic analysis of this compensator leads to Figures 8-11, where the CDF of the dominant closed-loop poles, the output, the control and the loop gain processes are displayed. Better robust stability characteristics, i.e., smaller values of $\bar{r}_\lambda(0)$, in this compensator are attained by increasing $\mathbf{w}_{(1)}$. Recall that reaching zero probability of instability might be unfeasible. From Figure 10 we see that for all possible parameter values and initial conditions the process $u(t)$ stays within the ± 0.5 range with more than 0.8 probability after 6 seconds. Figure 11 shows that uncertainty mostly affects the damping and the location of the resonant frequency. While all the percentiles for $\omega < 0.1$ are indistinguishable from the nominal curve, percentiles in the $\omega \in [0.1, 1]$ are not shown. In contrast to the mid frequency range, where the effects of uncertainty are large, there is no violation of the low frequency design requirement. The CDFs of λ for the nominal and the reliability based compensator are superimposed in Figure 12. Despite the increased variability of the dominant closed-loop poles of the reliability-based compensator (the support of λ is about two and a half times larger than the one for the nominal compensator), the system is robustly unstable with 3.13×10^{-4} probability. A substantial improvement in the performance is achieved by trading off a very small margin of the probability of stability. This improvement can be seen after comparing

Figures 6-7 with 9-10. Overall, the performance resulting from \mathbf{k}_2 is substantially better than the one resulting from \mathbf{k}_1 .

During optimization, 157 random variables were used to evaluate \mathbf{c} for the coarse assessment A_1 . This task took 23.6 seconds when performed on a Pentium III 1795 MHz with 512 MB of RAM. Notice that the CPU time associated with A_2 depends on the initial conditions used to find the MPPs. For this assessment, HSS was used for 628 random variables and the hybrid approach was used for robust stability. This task took 102 seconds.

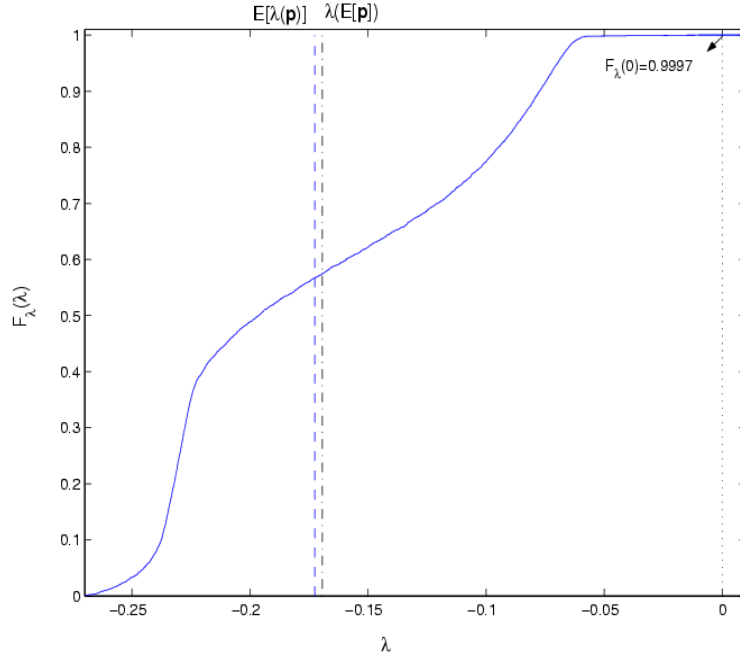


Figure 8. CDF of λ for the reliability-based optimal compensator.

7.1.3 Using Mean and Variance based metrics

If only means and variances are used, reliability and robustness metrics can be combined to form $\mathbf{c} = [\bar{b}_\lambda(0), \tau_{y(t)}(1), \tau_{u(t)}(0), \bar{b}_{q(\omega)}(1), \bar{b}_{q(\omega)}(0.75/\omega)]^T$. Ranges provided before will be used with the exception of $\omega \in [5, 10^2]$ for \bar{b} . All the components of the cost vector require of the estimation of means and variances, task that can be performed via sampling or the FSMSO method.

HSS leads to $\mathbf{k}_3 = 10^5[1.1207, 0.2307, 1.5235, 0.1713, 0.001, 0.0692, 1.2294, 1.069]^T$ and $\mathbf{c} = [8.6 \times 10^{-5}, 0.0057, 0.0129, 1.94 \times 10^{-4}, 6.189 \times 10^{-5}]^T$ for which the weighting vector $\mathbf{w} = [500, 1, 4, 1, 1]^T$ was used. A probabilistic analysis of this compensator leads to the results shown in Figures 13, 14 and 15. Figure 13 shows that the optimal compensator makes λ insensitive to uncertainty, i.e. the CDF resembles a step function which would result if the system is deterministic. Notice that the bound on the stability condition tends to reduce the variability of λ . This artificially reduces

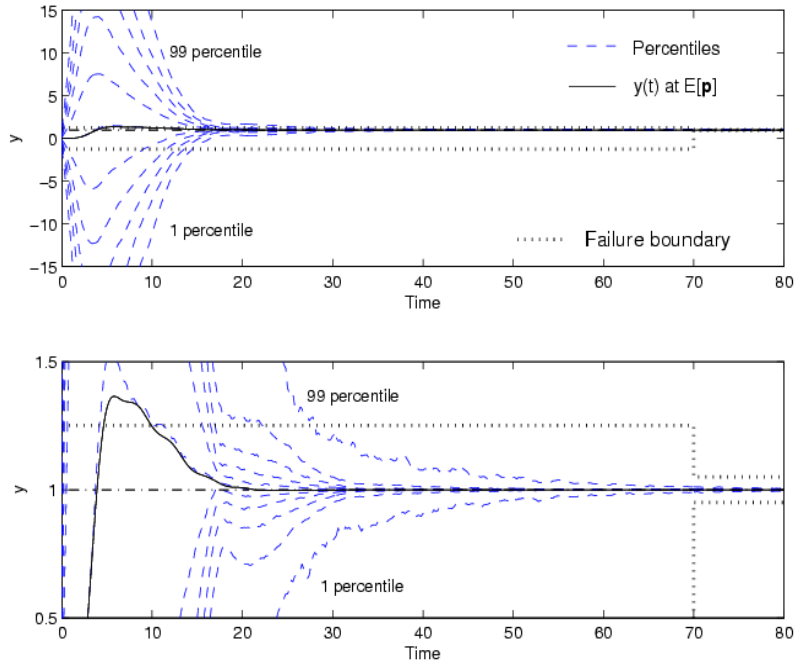


Figure 9. $y(t)$ for the reliability-based optimal compensator. A zoom is shown below.

the design space, i.e. there might exist solutions with a better performance in which large variances in λ occur. This is a consequence of the form of the bound. The comparison between the time responses for the reliability compensator and Figures 14 and 15 show substantial differences between the two solutions. While the control for the reliability based compensator intends to keep the process within the strip $|u| < 0.5$, the mean and variance based solution intends to concentrate the random process about the target function $\hat{u} = 0$. It can be seen that this is achieved by inducing oscillations about the target function. The reader should also notice that excursions beyond the failure boundaries in a reliability formulation, e.g. $y(t)$ in Figure 9 for the first 10 seconds, are not penalized according to the severity of the violation. This is in sharp contrast with the mean and variance formulation. Since we are using the same number of samples as before, the savings in CPU time when comparing this formulation with the one of the previous section result from not using FORM. Hence, the CPU time for A_1 is about the same while the CPU time for A_2 is 77s. For a given number of samples, the estimation of means and variances is in general more accurate than the estimation of failure probabilities. Small sample sets however, result in larger estimation errors of the moments, which could lead to the selection of the wrong conditions in Equations (19-20) and (22-23).

Next, the FSMSO method is used for estimating the cost vector. The first and second order derivatives for all the metrics of interest, i.e., closed-loop poles, output, control and loop transfer function, were derived analytically. Some of the required

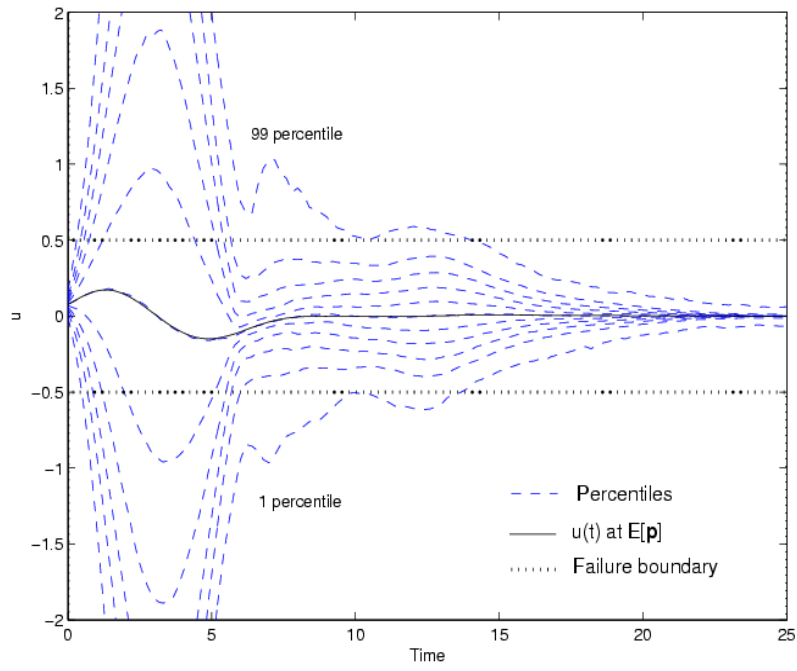


Figure 10. $u(t)$ for the reliability-based optimal compensator.

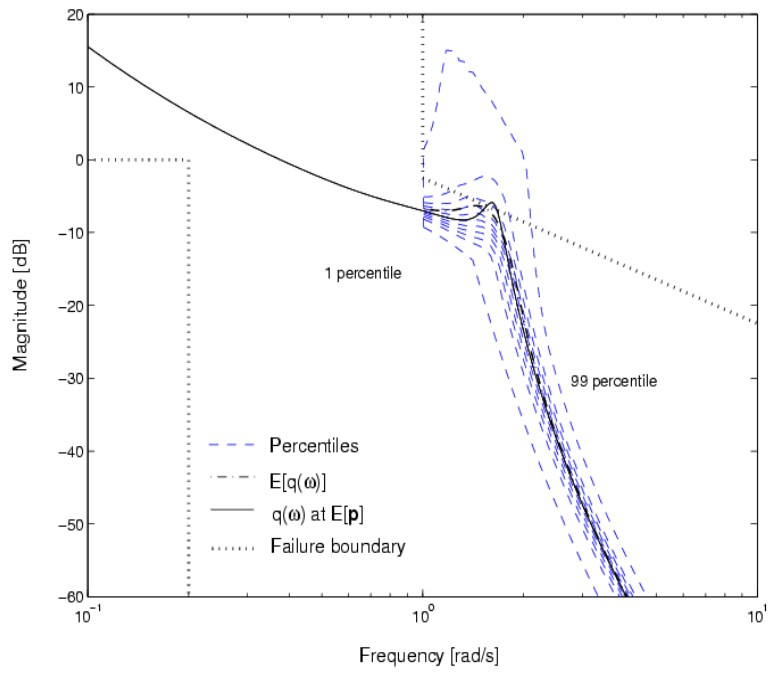


Figure 11. Bode plot of the loop gain for the reliability-based optimal compensator.

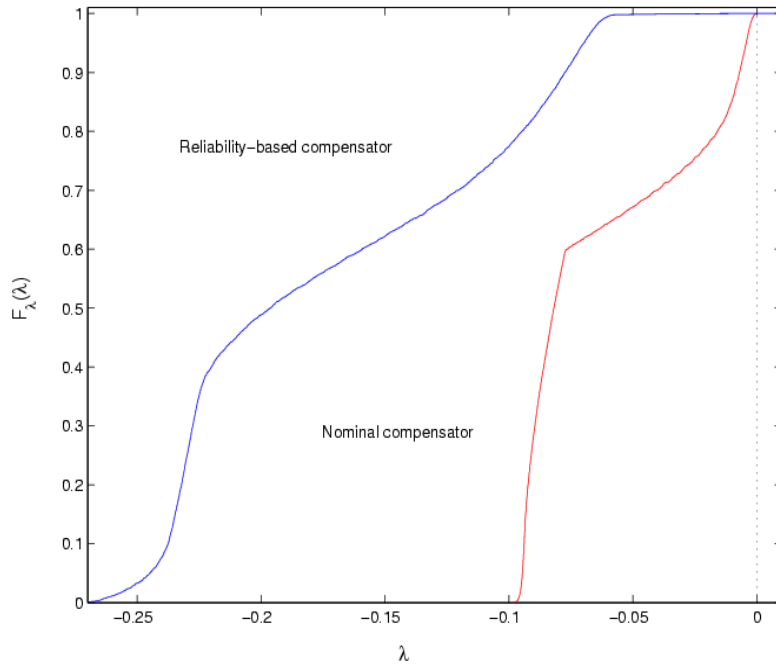


Figure 12. CDFs of λ .

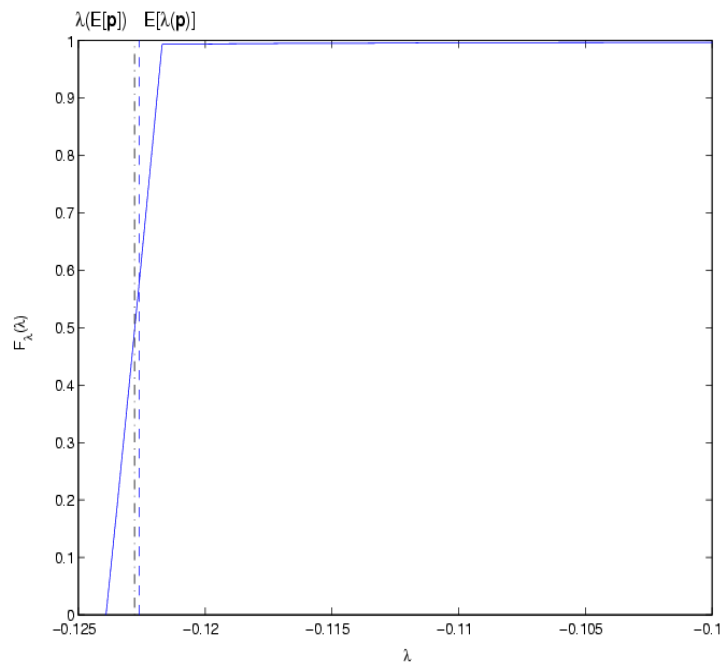


Figure 13. CDF of λ for the mean and variance based compensator.

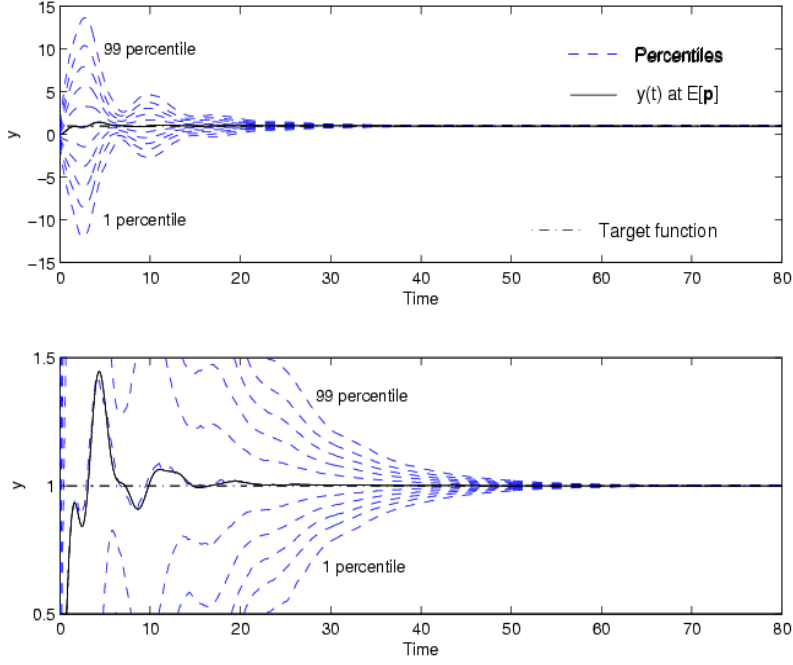


Figure 14. $y(t)$ for the mean and variance based compensator. A zoom is shown below.

expressions are as follows

$$\begin{bmatrix} \dot{\tilde{\mathbf{x}}} \\ \partial \dot{\tilde{\mathbf{x}}} \\ \partial^2 \dot{\tilde{\mathbf{x}}} \end{bmatrix} = \begin{bmatrix} \tilde{\mathbf{A}} & \mathbf{0} & \mathbf{0} \\ \partial \tilde{\mathbf{A}} & \tilde{\mathbf{A}} & \mathbf{0} \\ \partial^2 \tilde{\mathbf{A}} & 2\partial \tilde{\mathbf{A}} & \tilde{\mathbf{A}} \end{bmatrix} \begin{bmatrix} \tilde{\mathbf{x}} \\ \partial \tilde{\mathbf{x}} \\ \partial^2 \tilde{\mathbf{x}} \end{bmatrix} + \begin{bmatrix} \tilde{\mathbf{B}} \\ \partial \tilde{\mathbf{B}} \\ \partial^2 \tilde{\mathbf{B}} \end{bmatrix} u \quad (37)$$

$$\begin{bmatrix} \tilde{\mathbf{y}} \\ \partial \tilde{\mathbf{y}} \\ \partial^2 \tilde{\mathbf{y}} \end{bmatrix} = \begin{bmatrix} \tilde{\mathbf{C}} & \mathbf{0} & \mathbf{0} \\ \partial \tilde{\mathbf{C}} & \tilde{\mathbf{C}} & \mathbf{0} \\ \partial^2 \tilde{\mathbf{C}} & 2\partial \tilde{\mathbf{C}} & \tilde{\mathbf{C}} \end{bmatrix} \begin{bmatrix} \tilde{\mathbf{x}} \\ \partial \tilde{\mathbf{x}} \\ \partial^2 \tilde{\mathbf{x}} \end{bmatrix} \quad (38)$$

where $\tilde{\mathbf{A}}$, $\tilde{\mathbf{B}}$, $\tilde{\mathbf{C}}$, and $\tilde{\mathbf{D}}$ were given in Equations (4) and (5), $\tilde{\mathbf{x}} = [\mathbf{x}_c^T, \mathbf{x}^T]^T$, $\partial[\cdot]$ indicates a derivative with respect to $\mathbf{p}_{(i)}$ excluding initial conditions, and

$$\tilde{\mathbf{A}} \triangleq \begin{bmatrix} \mathbf{A}_c & -\mathbf{B}_c \mathbf{C} \\ \mathbf{B} \mathbf{C}_c & \mathbf{A} - \mathbf{B} \mathbf{D}_c \mathbf{C} \end{bmatrix},$$

$$\partial \tilde{\mathbf{A}} = \begin{bmatrix} \mathbf{0} & -\mathbf{B}_c \partial \mathbf{C} \\ \partial \mathbf{B} \mathbf{C}_c & \partial \mathbf{A} - \mathbf{B} \mathbf{D}_c \partial \mathbf{C} - \partial \mathbf{B} \mathbf{D}_c \mathbf{C} \end{bmatrix},$$

$$\partial^2 \tilde{\mathbf{A}} = \begin{bmatrix} \mathbf{0} & -\mathbf{B}_c \partial^2 \mathbf{C} \\ \partial^2 \mathbf{B} \mathbf{C}_c & \partial^2 \mathbf{A} - \mathbf{B} \mathbf{D}_c \partial^2 \mathbf{C} - 2\partial \mathbf{B} \mathbf{D}_c \partial \mathbf{C} - \partial^2 \mathbf{B} \mathbf{D}_c \mathbf{C} \end{bmatrix},$$

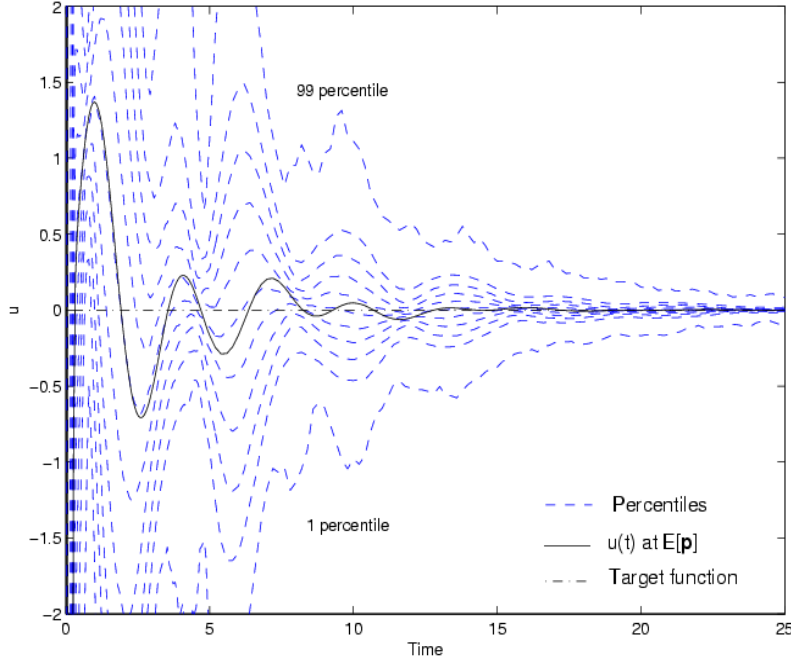


Figure 15. $u(t)$ for the mean and variance base compensator

$$\tilde{\mathbf{B}} \triangleq [\mathbf{B}_c \quad \mathbf{B}\mathbf{D}_c]^T, \partial\tilde{\mathbf{B}} = [\mathbf{0} \quad \partial\mathbf{B}\mathbf{D}_c]^T, \partial^2\tilde{\mathbf{B}} = [\mathbf{0} \quad \partial^2\mathbf{B}\mathbf{D}_c]^T,$$

$$\tilde{\mathbf{C}} \triangleq [\mathbf{0} \quad \mathbf{C}], \partial\tilde{\mathbf{C}} = [\mathbf{0} \quad \partial\mathbf{C}], \partial^2\tilde{\mathbf{C}} = [\mathbf{0} \quad \partial^2\mathbf{C}]$$

In these expressions, the subscript c refers to the state space representation of the compensator K while the matrices with no subscript refer to the open-loop plant. The time evolution of the sensitivities is calculated by solving the state space model in Equations (37-38). Sensitivities with respect to initial conditions can be analytically calculated via the matrix exponential. Such developments as well as the ones for the other sensitivities are omitted due to space limitations. In general, the analyses based on FSMSO were inaccurate when compared with sampling. Even though the CPU time per analysis was reduced to 2 seconds, large errors in the estimation precluded its use for synthesis. Table 2 shows a comparison between the assessments resulting from HSS and FSMSO as the variance of the uncertain parameters is increased. The same PDFs for the input uncertainty of Table 1 are used while the means are kept constant. The right most column shows the average relative error in the components of \mathbf{c} . For the Beta distributions, the increase of the variance was attained by enlarging the support. The terms resulting from the crossed derivatives were neglected. It can be observed that the accuracy of the FSMSO estimation rapidly decreases as $f_{\mathbf{p}}(\mathbf{p})$ is less concentrated about its mean. This trait is obvious since large excursions from $\mathbf{E}[\mathbf{p}]$ might considerably degrade the accuracy of the Taylor approximation.

Table 2. Comparison of HSS and FSMSO for \mathbf{k}_3 .

$V[\mathbf{p}_{(i)}]$ for $i = 1, \dots, 7$	Cost vector \mathbf{c}	Average error
1×10^{-4}	$\mathbf{c}_{HSS} = 10^{-3}[0.000823, 0.0096, 0.5880, 0.0058, 0.0013]$ $\mathbf{c}_{FSMSO} = 10^{-3}[0.000827, 0.0095, 0.5880, 0.0058, 0.0001]$	0.3%
1×10^{-3}	$\mathbf{c}_{HSS} = 10^{-3}[0.00824, 0.0110, 0.6560, 0.0580, 0.0136]$ $\mathbf{c}_{FSMSO} = 10^{-3}[0.00823, 0.0108, 0.7720, 0.0580, 0.0133]$	4%
3×10^{-3}	$\mathbf{c}_{HSS} = 10^{-3}[5.1000, 0.0505, 0.8800, 0.1745, 0.0446]$ $\mathbf{c}_{FSMSO} = 10^{-3}[0.0247, 0.0194, 1.9160, 0.1740, 0.0408]$	57%
4×10^{-3}	$\mathbf{c}_{HSS} = 10^{-3}[32.400, 0.0013, 1.0880, 0.2330, 0.0626]$ $\mathbf{c}_{FSMSO} = 10^{-3}[0.0329, 0.0267, 2.8680, 0.2320, 0.0548]$	454%

To show the reduction in the design space caused by using $\bar{b}_\lambda(0)$, we have solved this problem using $\bar{r}_\lambda(0)$ instead. This practice results in the compensator $\mathbf{k}_4 = 10^5[0.9082, 0.3590, 1.1773, 0.2372, 0.001, 0.0616, 1.0432, 1.196]^T$ for which $\mathbf{c} = [1.86 \times 10^{-5}, 0.0052, 0.0121, 1.845 \times 10^{-4}, 6.10 \times 10^{-5}]^T$. Figure 16 shows that Δ_λ is about 10 times larger than the one in Figure 13. Actually, $V[\lambda]$ is about 2276 times larger. This fact heavily penalizes the compensator via $\bar{b}_\lambda(0)$ in spite of its actual improved performance. The reader should also notice that there is an offset of about 10% between $E[\lambda(\mathbf{p})]$ and $\lambda(E[\mathbf{p}])$. Performance improvements in all the metrics were attained. Figures 17 and 18 show the corresponding output and control, from which considerable improvements are seen when compared with Figures 14 and 15.

7.2 Disturbance Rejection for a Flexible Beam

The second example will focus on the disturbance rejection for a flexible beam test article with both physical and modal parameter uncertainties. The system, displayed in Figure 19, consists of a flexible thin aluminum blade, one-meter long, attached at its base to a hub motor. The hub motor is the control actuator for the system. At the tip of the beam, there is a reaction wheel that serves as a disturbance generator. The test article has nine sensors that may be used in any combination for either feedback or performance output monitoring. The finite element method is used to model this system by utilizing Euler-Bernoulli planar beam elements. A complete description of the flexible beam test article [20] is available.

For this paper a SISO system is studied. The input \mathbf{u} is the hub motor torque and the measured output \mathbf{y} is the tip velocity. The tip reaction wheel disturbance is modeled by passing a Gaussian white noise process through a second-order linear low-pass filter, with parameters $\xi_f = 0.8$ and $\omega_f = 200\pi$ rad/s. The first five modes of the elastic structure are used to build a state space realization of the plant. This, in addition to the disturbance model leads to an open-loop system where $\mathbf{x} \in \mathbb{R}^{12}$, $\mathbf{u} \in \mathbb{R}$ and $\mathbf{y} \in \mathbb{R}$. The uncertain parameters are the Young's Modulus E (Pa), the density ρ (Kg/m³) and the damping ratios of the retained vibration modes ξ_i , $i = 1, 2, 3, 4, 5$. This set leads to $\mathbf{p} = [E, \rho, \xi_1, \xi_2, \xi_3, \xi_4, \xi_5]^T$, whose components are assumed independent. The corresponding PDFs are given in Table 3. The mean

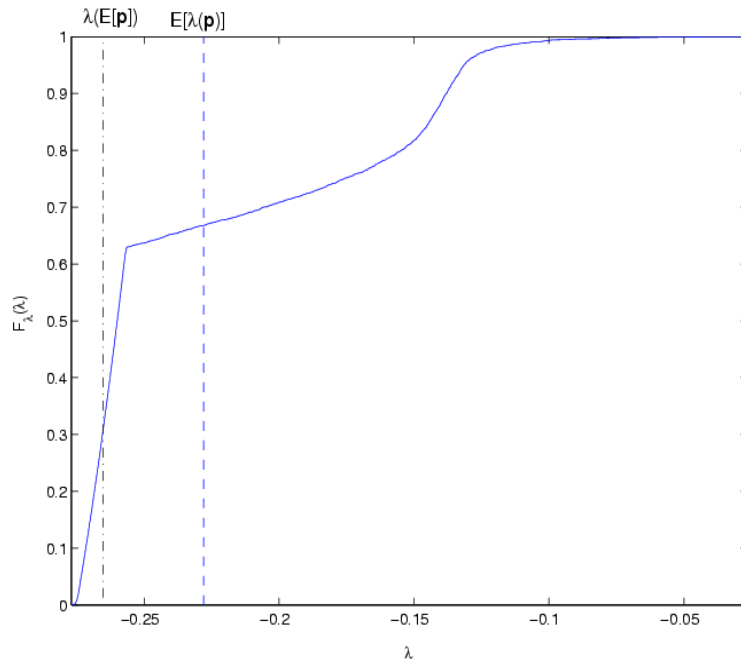


Figure 16. CDF of λ for a compensator with parameters \mathbf{k}_4 .

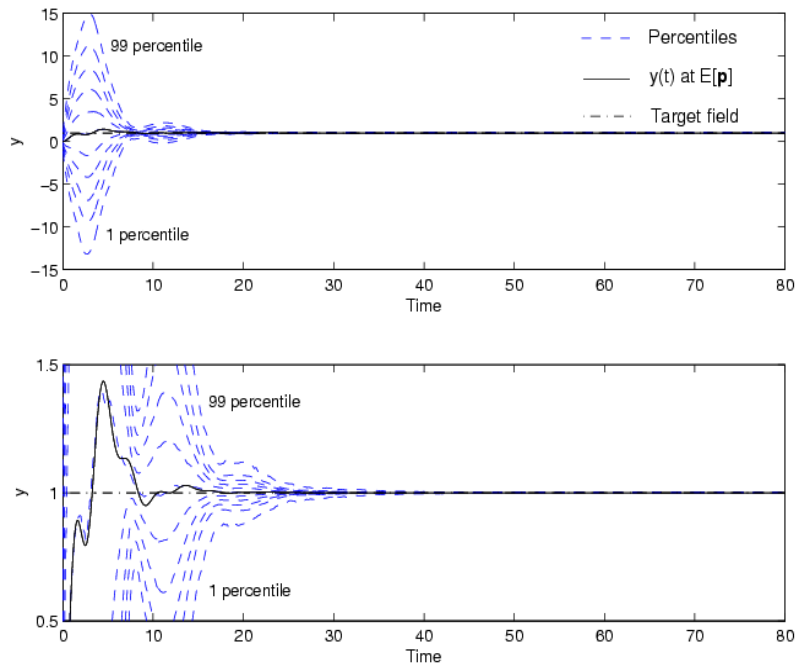


Figure 17. $y(t)$ for a compensator with parameters \mathbf{k}_4 . A zoom is shown below.

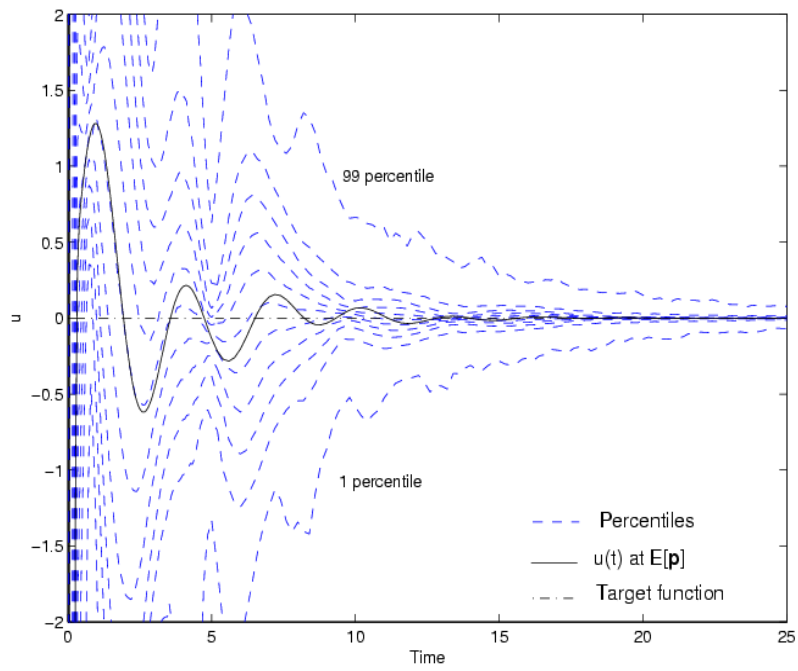


Figure 18. $u(t)$ for a compensator with parameters \mathbf{k}_4

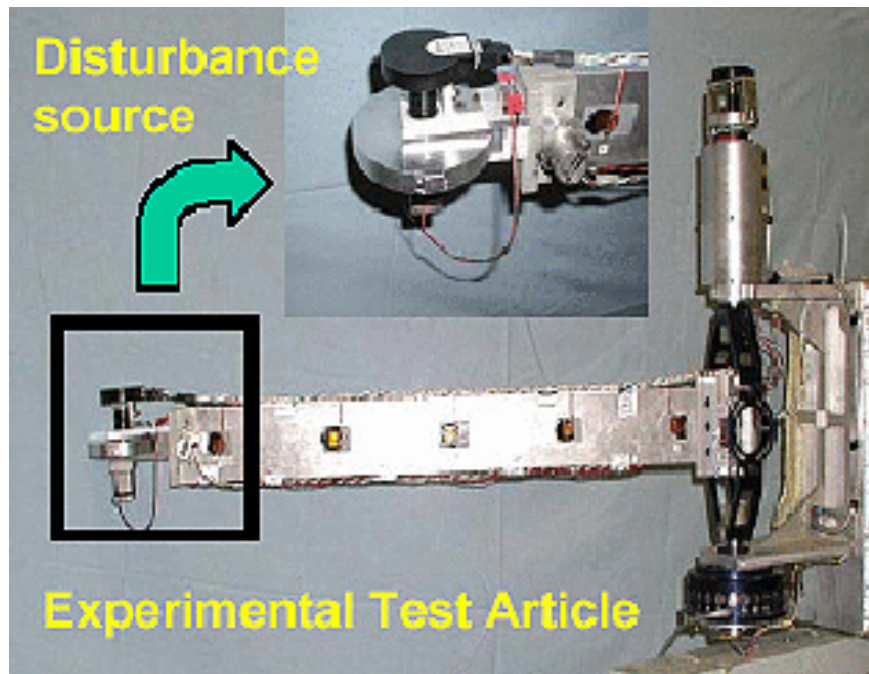


Figure 19. Flexible beam test article.

Table 3. Uncertainty Model.

E	$\Delta_E = 10^{10}[5.226, 7.839]$	$f_E(E) = B(5, 5)$
ρ	$\Delta_\rho = [2280, 3420]$	$f_\rho(\rho) = B(3, 3)$
ξ_1	$\Delta_{\xi_1} = [0.08, 0.12]$	$f_{\xi_1}(\xi_1) = B(2, 2)$
ξ_2	$\Delta_{\xi_2} = [0.0252, 0.0378]$	$f_{\xi_2}(\xi_2) = B(2, 2)$
ξ_3	$\Delta_{\xi_3} = [0.02, 0.03]$	$f_{\xi_3}(\xi_3) = B(2, 2)$
ξ_4	$\Delta_{\xi_4} = [0.0304, 0.0456]$	$f_{\xi_4}(\xi_4) = B(2, 2)$
ξ_5	$\Delta_{\xi_5} = [0.02, 0.03]$	$f_{\xi_5}(\xi_5) = B(2, 2)$

values of the uncertain parameters are set to coincide with parameters in the finite element model leading to good matches with experimental data. The supports of the distributions were set according to reasonable ranges of variation. The shapes of the PDFs were chosen arbitrarily. Performance requirements on stability and the output RMS are considered. Full-state feedback with a full-order observer determine the control structure.

7.2.1 Nominal Compensator

As before, a baseline compensator for the nominal plant is designed such that the RMS value is minimized. The resulting compensator, with parameters \mathbf{d}_1 , leads to $y_{rms} = 0.011$ m/s. The propagation of the uncertainty prescribed in Table 3 through the closed loop-system show that this compensator is robustly unstable with $\bar{r}_\lambda(0) = 0.235$.

7.2.2 Reliability-based Compensator

For this example, a shapable failure domain for the RMS requirement is assumed. This leads to the cost vector $\mathbf{c} = [\bar{r}_\lambda(0), \bar{r}_{y_{rms}}(\mathbf{e}) + \gamma_{y_{rms}}]^T$, where $\mathbf{e} \in [0, 0.05]$ and $\gamma_{y_{rms}} = \mathbf{e}$. The selected control structure makes the feedback gain \mathbf{G} , the observer gain \mathbf{L} and the RMS failure boundary \mathbf{e} , the design variables. Recall that the separation principle does not hold. The resulting closed-loop dynamics is given by Equations (4) and (5). Notice that although the observer is deterministic, all the closed-loop poles are random.

The synthesis approach with $\mathbf{w} = [20, 1]^T$ leads to a compensator with parameters \mathbf{d}_2 , for which $\bar{r}_\lambda(0) = 0$, $\mathbf{e} = 0.0139$ m/s, $\bar{r}_{y_{rms}}(\mathbf{e}) = 3.6 \times 10^{-3}$ and $\mathbf{c} = [0, 3.6 \times 10^{-3}]^T$. The probabilistic analysis of this compensator leads to the results shown in Figures 20-21. Figure 20 shows that the random variable y_{rms} for \mathbf{d}_2 is moved toward zero from $\bar{y}_{rms} = 0.05$, by virtue of the non-fixed failure boundary. Figure 21 shows Bode magnitude plots of the disturbance to output transfer function, namely T_{zy} . Notice that differences in the mid-frequency range, i.e. $\omega \approx 1$, of the diagram have a bigger impact on the RMS value. In addition, considerable variability in the closed-loop Bode magnitude plot as well as a significant reduction in the damping of the first mode are attained near 20 rad/s. It is interesting to notice that even though \mathbf{d}_2 leads to a robustly stable closed-loop system in Equation (4),

the full-state feedback subsystem $\tilde{\mathbf{A}}_{1,1}$ and the full-order observer subsystem $\tilde{\mathbf{A}}_{2,2}$ have a non-zero probability of instability. This indicates that the application of the Separation Principle before accounting for uncertainty in the model artificially reduces the design space. In other words, a design that accommodates for uncertainty based on the full system dynamics, i.e. Equation (4), may lead to robustly stable solutions in a design region which would have been rejected for reasons of instability if the Separation Principle had been applied before searching for a robust regulator with full-state feedback and a robust observer.

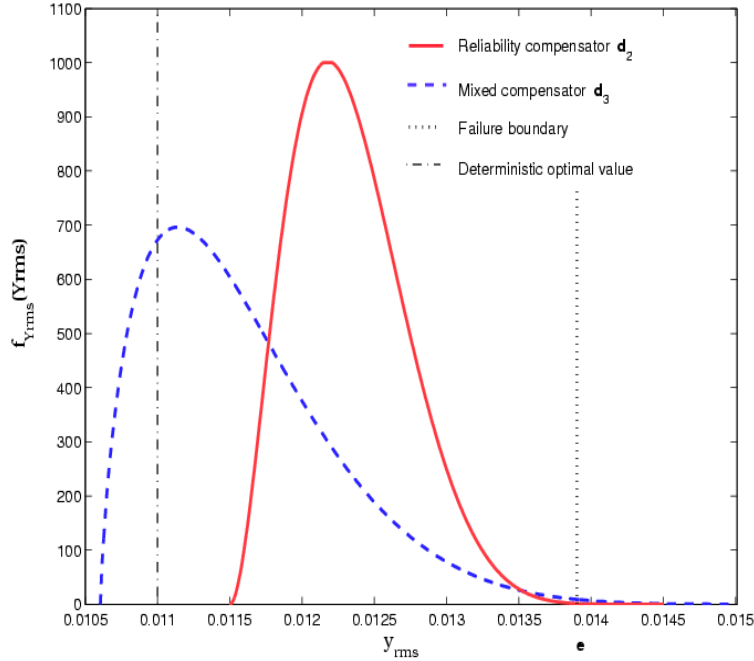


Figure 20. PDFs for the reliability based and the robustness based compensators.

7.2.3 Mixed Compensator

Lets take $\mathbf{c} = [\bar{r}_\lambda(0), \tau_{y_{rms}}(0)]^T$, where the hybrid approach will be used for the stability metric and HSS for the RMS metric. The synthesis algorithm leads to \mathbf{d}_3 , for which $\mathbf{c} = [0, 1.34 \times 10^{-4}]^T$. This compensator leads to the dashed line in Figure 20. Comparing both solutions, we see that while the PDF corresponding to the reliability-based compensator has less probability of exceeding the boundary value of $\mathbf{e} = 0.0139$ m/s, the robustness-based compensator leads to a PDF which is much more concentrated toward the ideal value of zero. This clearly shows that the conceptual differences between the two formulations. Since there is no conservatism in the selection of the nominal plant, i.e., $G(\mathbf{E}[\mathbf{p}])$ is not the most difficult plant to control, $y_{rms} = 0.011$ m/s does not necessarily bound the supports of the PDFs. This can be observed in Figure 20, where the support corresponding to \mathbf{d}_3 contains $y_{rms} = 0.011$ m/s.

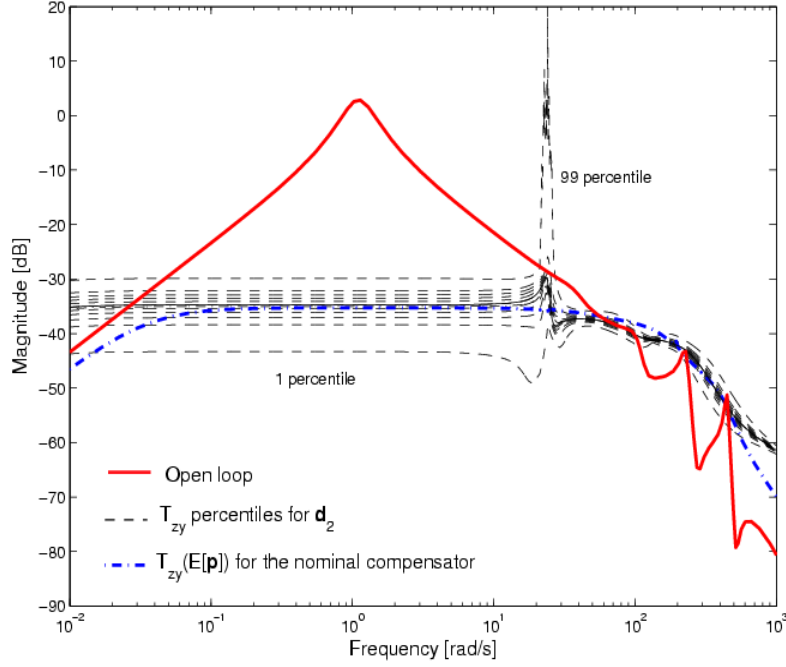


Figure 21. Bode diagrams of T_{zy} for \mathbf{d}_2 .

7.2.4 Mean and Variance based Compensator

For this case we assume $\mathbf{c} = [\bar{b}_\lambda(0), \tau_{y_{rms}}(0)]^T$, where the FSMSO method will be used to estimate both indexes. In contrast to the previous example, the accuracy of the results made the method suitable for synthesis. Analytical sensitivities were used in the moments approximations. For instance, the sensitivities of the closed-loop poles that determine λ are given by

$$\begin{aligned}\tilde{\mathbf{A}}\mathbf{v}_j &= s_j\mathbf{v}_j \\ \partial s_j &= \mathbf{z}_j^T \partial \tilde{\mathbf{A}} \mathbf{v}_j \\ \partial^2 s_j &= \mathbf{z}_j^T \left[\partial^2 \tilde{\mathbf{A}} + (\partial \tilde{\mathbf{A}} - \partial s_j \mathbf{I})(s_j \mathbf{I} - \tilde{\mathbf{A}})^{-1} \partial \tilde{\mathbf{A}} + \partial \tilde{\mathbf{A}}(s_j \mathbf{I} - \tilde{\mathbf{A}})^{-1} (\partial \tilde{\mathbf{A}} - \partial s_j \mathbf{I}) \right] \mathbf{v}_j\end{aligned}$$

where \mathbf{z}_j is the j th eigenvector of $\tilde{\mathbf{A}}^T$, the right and left eigenvalues are normalized, i.e. $\mathbf{z}_j^T \mathbf{v}_j = 1$, and non-repeated poles are assumed. Derivatives of the output covariance are given by

$$\partial \tilde{\mathbf{y}}_{rms} = \left\{ \text{diag} \left[\tilde{\mathbf{C}} \partial \mathbf{Q} \tilde{\mathbf{C}}^T + 2 \partial \tilde{\mathbf{C}} \mathbf{Q} \tilde{\mathbf{C}}^T \right] \right\}^{1/2}$$

$$\partial^2 \tilde{\mathbf{y}}_{rms} = \left\{ \text{diag} \left[\tilde{\mathbf{C}} \partial^2 \mathbf{Q} \tilde{\mathbf{C}}^T + 4 \partial \tilde{\mathbf{C}} \partial \mathbf{Q} \tilde{\mathbf{C}}^T + 2 \partial^2 \tilde{\mathbf{C}} \mathbf{Q} \tilde{\mathbf{C}}^T + 2 \partial \tilde{\mathbf{C}} \partial \mathbf{Q} \partial \tilde{\mathbf{C}}^T \right] \right\}^{1/2}$$

where the derivatives of the state covariance are given by the solution to the set of Lyapunov equations

$$\tilde{\mathbf{A}} \partial \mathbf{Q} + \partial \mathbf{Q} \tilde{\mathbf{A}}^T + \partial \tilde{\mathbf{A}} \mathbf{Q} + \mathbf{Q} \partial \tilde{\mathbf{A}}^T + \partial \tilde{\mathbf{B}} \tilde{\mathbf{S}}^T + \tilde{\mathbf{B}} \mathbf{S} \partial \tilde{\mathbf{B}}^T = 0$$

$$\begin{aligned} & \tilde{\mathbf{A}}\partial^2\mathbf{Q} + \partial^2\mathbf{Q}\tilde{\mathbf{A}}^T + 2\partial\tilde{\mathbf{A}}\partial\mathbf{Q} + 2\partial\mathbf{Q}\partial\tilde{\mathbf{A}}^T + \partial^2\tilde{\mathbf{A}}\partial\mathbf{Q} + \\ & \partial\mathbf{Q}\partial^2\tilde{\mathbf{A}}^T + 2\partial\tilde{\mathbf{B}}\mathbf{S}\partial\tilde{\mathbf{B}}^T + \partial^2\tilde{\mathbf{B}}\mathbf{S}\tilde{\mathbf{B}}^T + \tilde{\mathbf{B}}\mathbf{S}\partial^2\tilde{\mathbf{B}}^T = 0 \end{aligned}$$

The synthesis algorithm leads to a compensator with parameters \mathbf{d}_4 , for which $\mathbf{c} = [5.33 \times 10^{-6}, 1.33 \times 10^{-4}]^T$. The resulting PDF for the RMS is indistinguishable from the one shown in Figure 20 even though the compensators are different. The CDFs of λ for \mathbf{d}_3 and \mathbf{d}_4 are superimposed in Figure 22. As before, the tendency of the formulation of making λ as deterministic as possible is apparent. Notice however, that the CPU time required for the analysis of \mathbf{d}_3 is 421 seconds while the one for \mathbf{d}_4 is 1.22 seconds. On the other hand, the analysis of the compensator with parameters \mathbf{d}_4 via HSS takes 64 seconds. This exemplifies substantial savings in CPU time which result from using the FSMSO method. In this example, those savings justify the labor required to compute analytical derivatives. The reader should recall, however, that the same method led to inaccurate results for the satellite example.

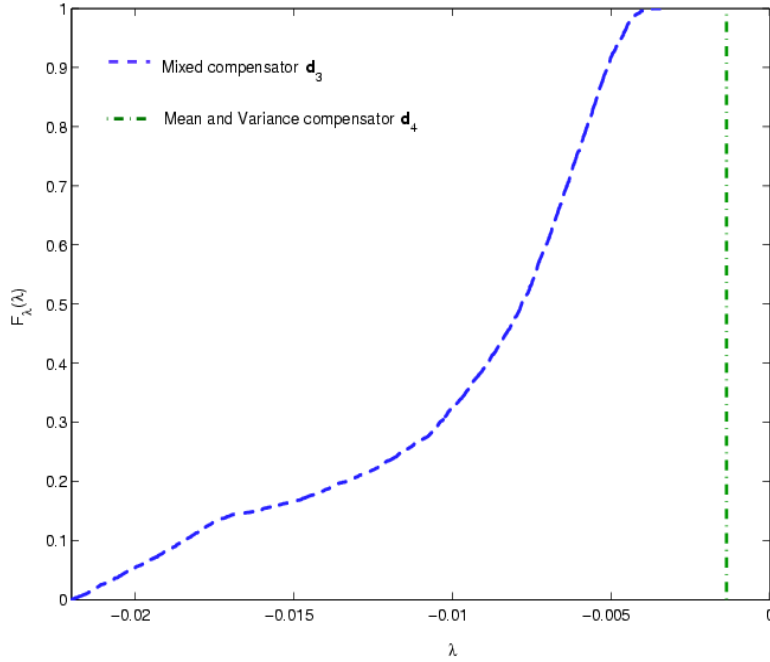


Figure 22. CDFs of λ for \mathbf{d}_3 and \mathbf{d}_4 .

8 Conclusions

This paper proposes a control synthesis methodology for systems with probabilistic uncertainty. Synthesis is performed by solving a multi-objective optimization problem which combines requirements of stability and performance in time- and frequency-domains. In this study, reliability- and robustness- based formulations are proposed and several numerical methods for estimation are examined. In a reliability formulation, the probability of violating design requirements is minimized

while admissible domains are contracted toward regions with an improved performance. In a robustness-based formulation, a metric that measures the concentration of the random variable/process about a target scalar/function is minimized. These two formulations lead to compensators with distinctive characteristics. In addition, metrics that bound the reliability metrics proposed, whose estimation only requires of means and variances, are also derived and used for control design.

Some of the fundamental differences between the proposed strategy and conventional robust control methods are: (i) unnecessary conservatism is eliminated since there is not need for convex supports/sets, (ii) the most likely plants are favored during synthesis allowing for probabilistic robust optimality, (iii) the tradeoff between robust stability and robust performance can be explored numerically, (iv) the uncertainty set, which could be unbounded, is closely related to parameters with clear physical meaning, and (v) compensators with improved robust characteristics for a given control structure can be designed, e.g., one can search for a PID controller with best robust characteristics. Examples related to the attitude control of a satellite and to control design for disturbance rejection in a flexible beam are used to demonstrate and validate the methodology.

References

1. Crespo, L. G.: Optimal performance, robustness and reliability based designs of systems with structured uncertainty. *Proceedings of American Control Conference*, Denver, CO USA, June 2003, vol. 5, pp. 4219–4224.
2. Laughlin, D. L.; Jordan, K. G.; and Morari, M.: Internal model control and process uncertainty - mapping uncertainty regions for SISO controller design. *International Journal of Control*, vol. 44, no. 6, December 1986, pp. 1675–1698.
3. Weinmann, A.: *Uncertain Models and Robust Control*. Springer-Verlag, New York, NY USA, 1991.
4. Zhou, K.; and Doyle, J. C.: *Essentials of Robust Control*. Prentice Hall, Upper saddle, New Jersey, 1998.
5. Marrison, C.; and Stengel, R.: Design of Robust Control Systems for a Hypersonic Aircraft. *Journal of Guidance, Control, and Dynamics*, vol. 21, January-February 1998, pp. 58–63.
6. Wang, Q.; and Stengel, R. F.: Robust Nonlinear Control of a Hypersonic Aircraft. *Journal of Guidance, Control, and Dynamics*, vol. 23, no. 4, July-August 2000, pp. 577–585.
7. Wang, Q.; and Stengel, R. F.: Searching for Robust Minimal-Order Compensators. *Journal of Dynamic Systems, Measurement and Control*, vol. 123, June 2001, pp. 233–236.
8. Calafiore, G.; Dabbene, F.; and Tempo, R.: Randomized Algorithms for Probabilistic Robustness with Real and Complex Structured Uncertainty. *IEEE Transactions on Automatic Control*, vol. 45, no. 12, December 2000, pp. 2218–2235.
9. Polyak, B.; and Tempo, R.: Probabilistic robust design with linear quadratic regulators. *Systems and Control Letters*, vol. 43, 2001, pp. 343–353.
10. Lagoa, C. M.; Li, X.; and Sznaier, M.: On the Design of Robust Controllers for Arbitrary Uncertainty Structures. *IEEE Transactions on Automatic Control*, vol. 48, no. 11, November 2003, pp. 2061–2065.
11. Spencer, B. F.; Sain, M. K.; Won, C-H.; Kaspari, D. C.; and Sain, P. M.: Reliability-based measures of structural control robustness. *Structural Safety*, vol. 15, 1994, pp. 111–129.
12. Rackwitz, R.: Reliability analysis, a review and some perspectives. *Structural Safety*, vol. 23, 2001, pp. 365–395.
13. Crespo, L. G.; and Kenny, S. P.: Reliability-based control design for uncertain systems. Accepted by the AIAA Journal of Guidance, Control, and Dynamics, 9/2/2004.

14. Wang, Q.; and Stengel, R. F.: Robust control of nonlinear systems with parametric uncertainty. *Automatica*, vol. 38, 2002, pp. 1591–1599.
15. Crespo, L. G.: Probabilistic formulations to robust optimal control. *45th AIAA Structures, Structural Dynamics and Materials Conference*, Palm Springs, CA USA, April 2004, pp. 1–21, AIAA Paper No. 2004-1667.
16. Skogestad, S.; and Postlethwaite, I.: *Multivariable feedback control*. John Wiley and Sons, Chichester, England, 1996.
17. Hokayem, P.; Abdallah, C.; and Dorato, P.: Quasi-Monte Carlo Methods in Robust Control Design. *IEEE Conference on Decision and Control*, Maui, HA USA, December 2003, pp. 2435–2440.
18. Kalagnanam, J. R.; and Diwekar, U. M.: An Efficient Sampling Technique for Off-line Quality Control. *Technometrics*, vol. 39, no. 3, August 1997, pp. 308–319.
19. Diwekar, U. M.; and Kalagnanam, J. R.: Efficient Sampling Technique for Optimization under Uncertainty. *American Institute of Chemical Engineering Journal*, vol. 43, no. 2, February 1997, pp. 440–447.
20. Kenny, Sean. P.: *Optimal rejection of nonstationary narrowband disturbances for flexible systems*. Ph.D. thesis, Massachusetts Institute of Technology, Cambridge, MA USA, February, 2002.

REPORT DOCUMENTATION PAGE				Form Approved OMB No. 0704-0188	
<p>The public reporting burden for this collection of information is estimated to average 1 hour per response, including the time for reviewing instructions, searching existing data sources, gathering and maintaining the data needed, and completing and reviewing the collection of information. Send comments regarding this burden estimate or any other aspect of this collection of information, including suggestions for reducing this burden, to Department of Defense, Washington Headquarters Services, Directorate for Information Operations and Reports (0704-0188), 1215 Jefferson Davis Highway, Suite 1204, Arlington, VA 22202-4302. Respondents should be aware that notwithstanding any other provision of law, no person shall be subject to any penalty for failing to comply with a collection of information if it does not display a currently valid OMB control number.</p> <p>PLEASE DO NOT RETURN YOUR FORM TO THE ABOVE ADDRESS.</p>					
1. REPORT DATE (DD-MM-YYYY) 01-03-2005		2. REPORT TYPE Technical Publication		3. DATES COVERED (From - To)	
4. TITLE AND SUBTITLE Robust Control Design for Systems With Probabilistic Uncertainty			5a. CONTRACT NUMBER		
			5b. GRANT NUMBER		
			5c. PROGRAM ELEMENT NUMBER		
6. AUTHOR(S) Crespo, Luis G.; Kenny, Sean P.			5d. PROJECT NUMBER		
			5e. TASK NUMBER		
			5f. WORK UNIT NUMBER 23-090-50-70		
7. PERFORMING ORGANIZATION NAME(S) AND ADDRESS(ES) NASA Langley Research Center Hampton, VA 23681-2199			8. PERFORMING ORGANIZATION REPORT NUMBER L-19084		
9. SPONSORING/MONITORING AGENCY NAME(S) AND ADDRESS(ES) National Aeronautics and Space Administration Washington, DC 20546-0001			10. SPONSOR/MONITOR'S ACRONYM(S) NASA		
			11. SPONSOR/MONITOR'S REPORT NUMBER(S) NASA/TP-2005-213531		
12. DISTRIBUTION/AVAILABILITY STATEMENT Unclassified-Unlimited Subject Category 08 Availability: NASA CASI (301) 621-0390					
13. SUPPLEMENTARY NOTES An electronic version can be found at http://ntrs.nasa.gov					
14. ABSTRACT This paper presents a reliability- and robustness-based formulation for robust control synthesis for systems with probabilistic uncertainty. In a reliability-based formulation, the probability of violating design requirements prescribed by inequality constraints is minimized. In a robustness-based formulation, a metric which measures the tendency of a random variable/process to cluster close to a target scalar/function is minimized. A multi-objective optimization procedure, which combines stability and performance requirements in time and frequency domains, is used to search for robustly optimal compensators. Some of the fundamental differences between the proposed strategy and conventional robust control methods are: (i) unnecessary conservatism is eliminated since there is not need for convex supports, (ii) the most likely plants are favored during synthesis allowing for probabilistic robust optimality, (iii) the tradeoff between robust stability and robust performance can be explored numerically, (iv) the uncertainty set is closely related to parameters with clear physical meaning, and (v) compensators with improved robust characteristics for a given control structure can be synthesized.					
15. SUBJECT TERMS Robust control, probabilistic uncertainty, optimality, reliability					
16. SECURITY CLASSIFICATION OF:			17. LIMITATION OF ABSTRACT	18. NUMBER OF PAGES	19a. NAME OF RESPONSIBLE PERSON
a. REPORT	b. ABSTRACT	c. THIS PAGE			STI Help Desk (email: help@sti.nasa.gov)
U	U	U	UU	53	19b. TELEPHONE NUMBER (Include area code) (301) 621-0390